Journal of Hydrology 542 (2016) 704–718

Contents lists available at ScienceDirect

Journal of Hydrology

journal homepage:www.elsevier.com/locate/jhydrd

Research papers

Island groundwater resources, impacts of abstraction and a drying climate: Rottnest Island, Western Australia

Eliza Bryan [a,b,c,⇑], Karina T. Meredith [b], Andy Baker [a,c], Vincent E.A. Post [d], Martin S. Andersen [a,e]

[a] Connected Waters Initiative Research Centre, UNSW Australia, Sydney, NSW 2052, Australia [b] Institute for Environmental Research, Australian Nuclear Science and Technology Organisation, Lucas Heights, NSW 2234, Australia [c] School of Biological, Earth and Environmental Sciences, UNSW Australia, Sydney, NSW 2052, Australia [d] School of the Environment/National Centre for Groundwater Research and Training, Flinders University, GPO Box 2100, Adelaide, SA 5001, Australia [e] School of Civil and Environmental Engineering, UNSW Australia, 2052 NSW, Australia

article info

Article history:
Received 11 March 2016
Received in revised form 15 September 2016
Accepted 17 September 2016
Available online 19 September 2016
This manuscript was handled by G. Syme, Editor-in-Chief

Keywords:
Island freshwater lens
Groundwater resources
Seawater intrusion
Climate change
Isotopes

abstract

Coastal aquifers provide a source of water for more than one billion people, with island freshwater lenses being some of the most vulnerable coastal groundwater systems due to their susceptibility to saltwater intrusion. Basic hydrogeological and hydrochemical knowledge regarding the recharge and salinisation processes of freshwater lenses is important to ensure sustainable utilisation, especially considering possible climate change effects. This paper makes an assessment of the fate of a freshwater lens in a drying climate through a comparison of current and historic hydrochemical data, which to the author's knowledge is unique to this study. Fresh groundwater stable isotope signatures ($\delta^{18}O$, $\delta^{2}H$) reflect local amount weighted rainfall signatures ($\delta^{18}O$: 3.8‰; $\delta^{2}H$: 15.1‰), and confirm rainfall as the origin of fresh groundwater ($\delta^{18}O$: 4.47 to 3.82‰; $\delta^{2}H$: 20.0 to 16.6‰). Mixing with seawater was identified through enriched groundwater $\delta^{18}O$ and $\delta^{2}H$ signatures (maximum values of 0.36‰ and 1.4‰ respectively) compared to local rainfall and higher salinity (maximum 29,267 mg/L Total Dissolved Solids (TDS)) in a number of monitoring wells around the freshwater lens. Enhanced seawater intrusion detected in the northern section of the lens area was identified through significantly increased TDS values over the last 20–40 years, with increases of up to 3000% observed between 1990 and 2014. A reduction in the extent of freshwater by approximately 1 km^2 was identified since 1977, which was found to be primarily caused by a reduction in recharge to the freshwater lens due to a 20% decline in winter rainfall in the south-west Western Australian region since the mid 1960s. Groundwater abstraction was found to equate to between 5% and 9% of the estimated recharge for the island, and is not a significant factor in the reduction of the lens extent compared to the observed decline in rainfall recharge. Interestingly, seawater intrusion into the fresh water lens was found to occur by older seawater (0.03–0.09 TU) in regions of the lens that were previously fresh or slightly brackish, while one sample (0.67 TU) suggests either modern seawater intrusion or mixing of older saline groundwaters (>60 years) with rainfall recharge. The use of tritium dating in this island aquifer was essential in identifying 'older' seawater that was previously unidentified until now. The isotopic and hydrochemical tools used in this paper quantify the effects of groundwater abstraction and climate variability on the freshwater lens and have implications for the sustainable management of the groundwater resource on Rottnest Island, and elsewhere.

around the world (Barlow, 2003; and references therein). The impacts of climate change on coastal aquifers is also of concern with global sea level rise (SLR) causing seawater intrusion (Nicholls et al., 2007), as well as a decline in recharge in areas of reduced rainfall and a subsequent decrease in the volume of freshwater available for utilisation (White and Falkland, 2010).

These issues are intensified on islands, where groundwater is often present in the form of a shallow freshwater lens according to the Ghyben–Herzberg principle (Ghyben, 1889; Herzberg, 1901), which involves fresh or brackish water 'floating' on more saline water due to density differences. On small carbonate islands, freshwater lenses are generally constrained to certain parts of the island, with the dominant controls on lens geometry being the size and shape of the island, as well as geologic variability (Cant and Weech, 1986; Vacher, 1997; Ritzi et al., 2001; Schneider and Kruse, 2003). Spatial patterns of elevation, surficial geomorphology, permeability and vegetation (Schneider and Kruse, 2003), as well as recharge source and tidal range (Ataie-Ashtiani et al., 1999) can also impact on freshwater lens geometry.

Freshwater lenses are particularly vulnerable to both natural and anthropogenic threats, due to their heavy reliance on rainfall recharge and the potential for contamination from human activities (White and Falkland, 2010). The global threat of seawater intrusion is well documented (Kinzelbach et al., 2003; Post, 2005; Barlow and Reichard, 2010) and is primarily associated with intensive groundwater abstraction (Yakirevich et al., 1998; Barlow, 2003; Barlow and Reichard, 2010),

1. Introduction

Coastal aquifers provide a source of water for the more than one billion people (Small and Nicholls, 2003), and come with a unique set of challenges when utilised as a potable water source. These systems are under increasing strain due to rapid population growth in coastal areas, combined with the small proportion of the global renewable water supply contained within these aquifers (Nicholls et al., 2007). Coastal aquifers contain the fresh-saline interface between terrestrial and oceanic hydrological systems (Taylor et al., 2013), with modern seawater intrusion occurring due to both natural and anthropogenic causes. Groundwater abstraction is one of the leading causes of salt water intrusion (Falkland, 1991), with cases of over-pumping well documented reduced rainfall and coastal topography (Oude Essink et al., 2010; Ferguson and Gleeson, 2012). Methods to investigate saltwater intrusion range from hydrochemical (Stuyfzand, 1999; Andersen et al., 2005; Appelo and Postma, 2005; Sivan et al., 2005) to geophysical (Fretwell and Stewart, 1981; Fitterman and Deszcz-Pan, 1998; Paine, 2003), with a recent review of seawater intrusion processes and investigations provided by Werner et al. (2013).

While the occurrence and principles of saltwater intrusion is well known, the number of well-characterised examples of saltwater intrusion remains small, limiting our understanding of its dynamics on real-world scales (Werner et al., 2013). Welldocumented cases of salt water intrusion therefore provide an important contribution to the body of literature surrounding the topic due to the uniqueness and complexities that surround each incidence of saltwater intrusion (Werner et al., 2013). Determining the causes of seawater intrusion is imperative for the sustainable utilisation and management of vulnerable groundwater resources. This study investigates a freshwater lens on a small carbonate island in south-west Western Australia which has been utilised as a potable water source since 1977. Groundwater abstraction on the Island peaks in the summer months (December-February) due to demand for water over the tourist season, which coincides with a period of little to no rainfall in the region. The long term viability of the lens has come into question due to declining rainfall in the region since the mid 1960s (Smith et al., 2000; Barria et al., 2015). Recent high-resolution global climate modelling suggests that rainfall will continue to decline in the region by approximately 40% from the 1911 to 1970 average by the late twenty-first century (Delworth and Zeng, 2014). Despite early studies which investigated the dimensions of the freshwater lens (Playford and Leech, 1977; Smith, 1982; Davidson and Mory, 1990; Hirschberg and Smith, 1990; Davidson, 1991; Playford, 1997), no further studies regarding the impacts of abstraction, a drying climate or tidal effects have been conducted to assess whether active salt water intrusion is impacting the geometry of the freshwater lens, and if so its exact causes. Understanding these aspects of the lens is vital for the effective utilisation and management of available water resources, particularly in light of the decreasing rainfall in the region.

This study aims to characterise the freshwater lens and mixing zone on a small carbonate island, through the analysis of groundwater levels and the hydrochemical and isotopic composition of rainwater, surface waters, seawater and groundwaters to confirm the origin of the groundwater, the current extent of the lens and identify seawater intrusion of either modern or older seawater. It also aims to identify temporal changes to the lens extent and variations in the volume of groundwater recharge since the 1970s by comparing the results to historic hydrochemical and rainfall data. This paper quantifies the effects of groundwater abstraction and climate variability on the freshwater lens extent and has implications for the sustainable management of the groundwater resources on small carbonate islands, both in Australia and elsewhere in the world.

2. Environmental setting

Rottnest Island is a small carbonate eolianite island located 18 km off the coast of Perth, Western Australia, and is part of the world's longest carbonate eolianite deposit (Brooke, 2001) (Fig. 1A and B). The island is an A-Class reserve under the Land Administration Act 1997, which provides the highest level of protection for public land in Western Australia and limits all activities which may disturb its environment. Rottnest Island is a wellknown Australian tourist destination, with approximately 500,000 visitors per year, which creates a significant demand for water resources on the island.

2.1. Climate

Rottnest Island has a Mediterranean type climate characterised by hot, dry summers and mild, wet winters. The island has a long term average rainfall of 691 mm/year (1880–2015) and an annual reference evapotranspiration (ET_o) of 1694 mm (Station Number 9038 and 9193) (BOM, 2016b). Rainfall in the south-west

⇑ Corresponding author at: Connected Waters Initiative Research Centre, UNSW Australia, Sydney, NSW 2052, Australia.
E-mail address: eliza.bryan@unsw.edu.au (E. Bryan).

http://dx.doi.org/10.1016/j.jhydrol.2016.09.043 0022-1694/ 2016

Western Australian region has been below average since the mid 1960s (Smith et al., 2000), with the cumulative rainfall residual (see Fig. 2 caption for a description) on Rottnest Island reflecting this trend (Fig. 2A). This has the potential to impact on the volume of freshwater available on Rottnest Island, as rainfall is the sole source of freshwater recharge to the aquifer.

2.2. Land use and vegetation

Rottnest Island has been used for various purposes since European settlement in the 1830s including as an aboriginal prison, for military training and agricultural purposes. In recent decades, as mentioned, it is primarily a tourist destination. The vegetation of Rottnest Island, which once covered an estimated 65% of the Island, has been heavily depleted by human activities and fire, with native forest and woodland cover reduced to 23% by 1941 and 5% by 1997 (Playford, 1997). The vegetation has also been impacted by native marsupials known as quokkas (Setonix brachyurus) (Rippey and Hobbs, 2003). The native flora of Rottnest Island consists of around 140 species, with the coast dominated by grasses including Spinifex sericeus and Westringia fruticosa (Gouramanis et al., 2012). Acacia rostelifera shrubs and three tree species (Melaleuca lanceolata, Callitris preissii and Pittosporum ligustrifolium) dominate the inland areas of the island (Rippey and Hobbs, 2003). Salt lakes that occur on the island are surrounded by various salt tolerant plants including species of Chenopodiaceae, Cyperaceae, Juncacaeae and Templetonia retusa (Gouramanis et al., 2012). Revegetation has commenced around the Island, however the area above the freshwater lens has been left generally free of trees to ensure maximum recharge to the freshwater lens.

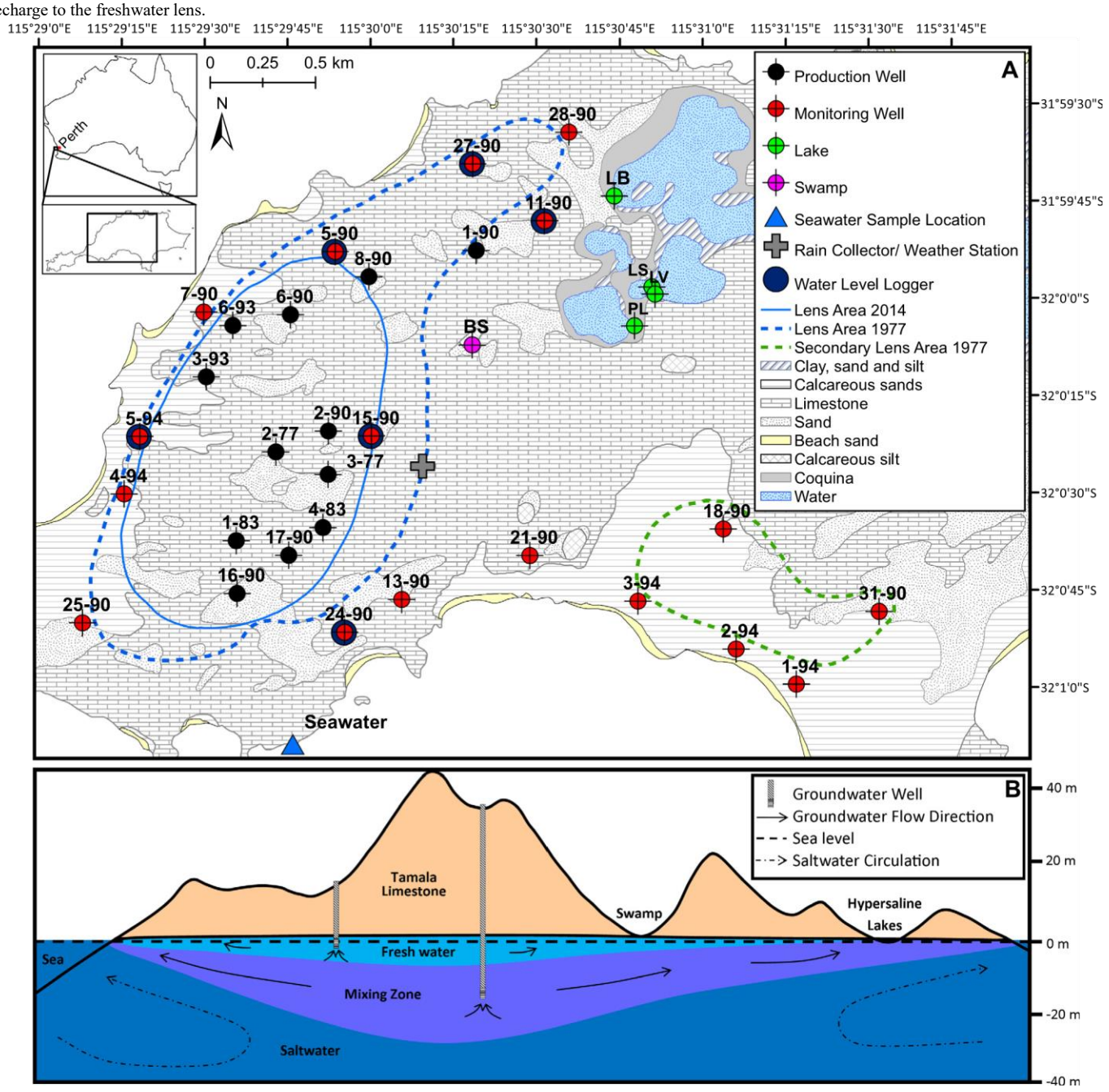

Fig. 1. (A) Location and geological map of the study area showing sample and water logger locations, weather station and rainfall collector location and the predicted lens areas in 1977 (adapted from Playford and Leech, 1977). The predicted reduction in the extent of the lens in 2014 compared to 1977 (insufficient data to assess secondary lens extent) is also shown. Surficial geology is based on

information provided by Gozzard (2011); and (B) a simplified east-west cross section of Rottnest Island, adapted from Smith (1985), showing groundwater flow directions and the circulation of seawater which is induced by the mixing of freshwater and saltwater in the mixing zone.

2.3. Geology and hydrogeology

Rottnest Island is 10.5 km long and up to 4.5 km wide, with a maximum elevation of 45 m Australian Height Datum (AHD). The Island is composed of Pleistocene to mid-Holocene carbonate eolianite (Tamala Limestone) with a total thickness of 115 m, of which around 70 m is below sea level (Playford and Leech, 1977). The Tamala limestone shows large scale eolian cross bedding and is typical of eogenetic karst of early to middevelopment, which forms through meteoric diagenesis (Vacher and Mylroie, 2002). The limestone is characterised by a large variability in hydraulic conductivity values of 100–2000 m/day and high matrix porosity (0.3–0.5) (Smith et al., 2012). The system in general is weakly cemented with abundant fossil root structures observed (Playford and Leech, 1977), and is typified by dual porosity consisting of numerous connected channels within a matrix of interparticle porosity (Smith et al., 2012). Diffuse dissolution of eolianites with large primary porosity leads to a diffuse-flow aquifer rather than one dominated by conduit flow, with a large transmissivity resulting from a welldeveloped dual-pore system, which increases the potential for rapid recharge (Smith et al., 2012). The island is similar to other carbonate eolianite islands such as Bermuda and the Bahamas, which are all characterised by dune shaped topography, large amplitude, high-angle cross-bedding, paleosols and fossiliferous marine units (Vacher, 1997).

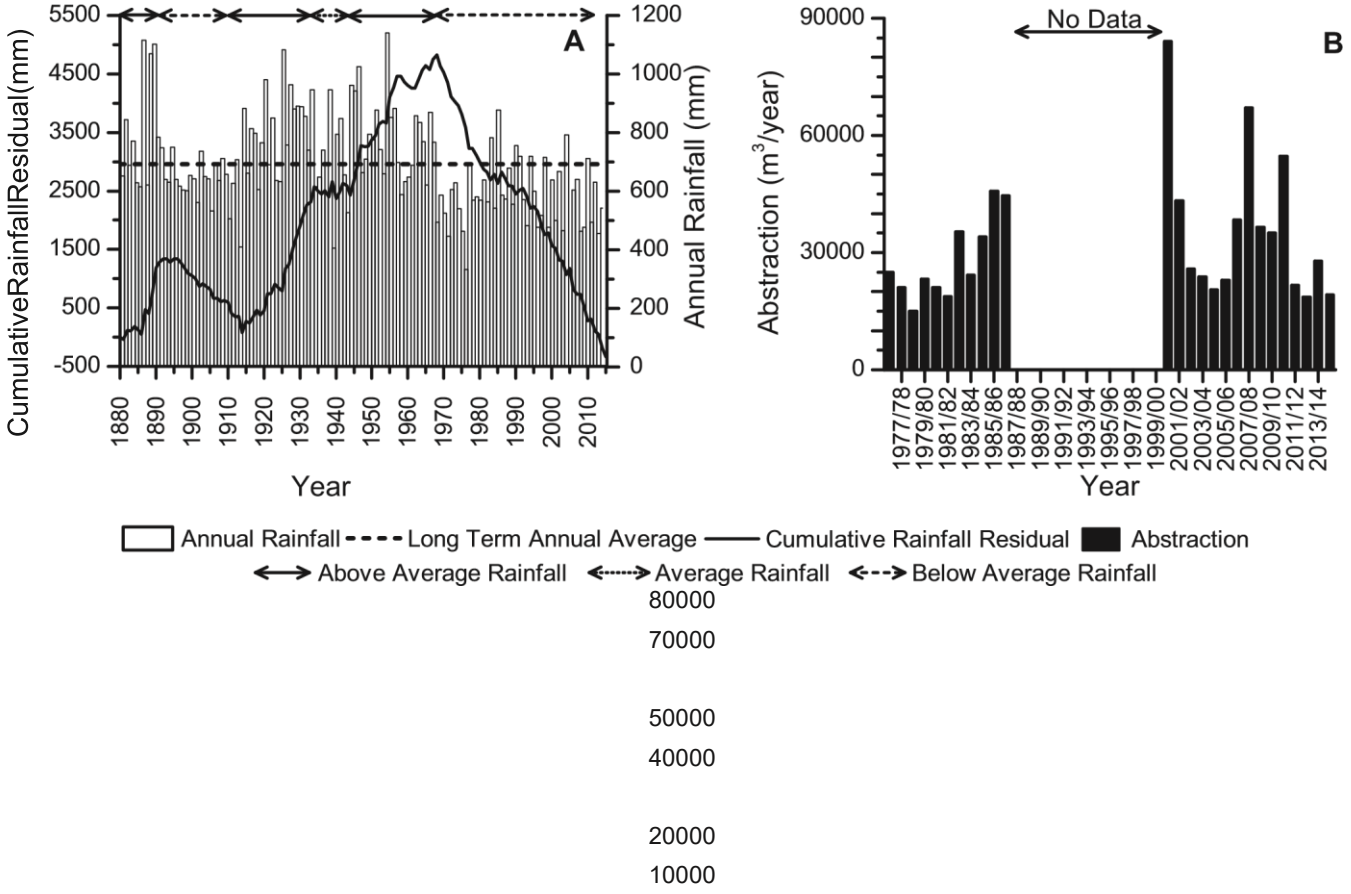

Fig. 2. (A) Annual rainfall and annual cumulative rainfall residual for Rottnest Island from 1880 to 2013, showing a period of below average rainfall from the mid 1960s to present (BOM, 2016b). The cumulative rainfall residual curve is calculated by subtracting the long term average annual rainfall from the recorded rainfall for a single year, and adding the difference to a rolling sum. A rising slope indicates a period of higher than average rainfall, while a falling slope indicates a period of lower than average rainfall; and (B) annual groundwater abstraction from the freshwater lens on Rottnest Island. Data is unavailable for the period 1987–2000.

Undulating hills and sand dunes characterise most of the Island, with an absence of water courses due to the highly permeable nature of the Tamala limestone. A number of permanent hypersaline lakes at or slightly below mean sea level are present and cover approximately 10% of the Island's surface area (Playford and Leech, 1977), as well as many lower salinity inter-dunal swamps (Edward and Watson, 1959; Edward, 1983). The lakes are believed to be partially filled remnants of "blue holes", which resulted from repeated carbonate deposition and dissolution cycles controlled by Quaternary sea level fluctuations (Mylroie et al., 1995), and closely resemble those of the Houtman Abrolhos reefs located 450 km north of Rottnest Island (Playford, 1988; Collins et al., 1991, 1993). Repeated evaporation of the lakes during summer, which were once connected to the sea, intensifies the observed hypersaline conditions (pre-summer 2014 TDS: 85,146 mg/L;

postsummer 2014 TDS: 336,610 mg/L (unpublished research)). While algal-cyanobacterial mats and mud sediments act as seals on the lake floors and prevent interaction with groundwater from below (Playford, 1997), limited discharge from the freshwater lens via seeps is observed around the perimeter of some lakes.

The freshwater lens on the Island is located within the upper section of the Tamala Limestone, with a mixing zone below reported to be more than 10 m thick (Edward and Watson, 1959; Playford and Leech, 1977) (Fig. 1B). Although there are no standard practices for defining the mixing zone, for the purpose of this paper the mixing zone is characterised by TDS values between 1000 mg/L and 35,000 mg/L (Barlow, 2003). The water table was previously suggested to be at a maximum of 0.5 m above sea level, with the freshwater extending to 8.5 m below sea level (Playford and Leech, 1977). The spatial extent of the freshwater lens was reported to have contracted significantly by the late 1970s due to a decline in precipitation since the mid-1960s (Playford and Leech, 1977), which occurred prior to the commencement of groundwater abstraction in 1977. A second, smaller freshwater lens is also present on the island, however it is not utilised for groundwater abstraction (Fig. 1A). Early investigations into the prevalence of fresh groundwater outside the lens perimeter and across the island found a thin layer of potable water which quickly turned brackish to saline on pumping (Playford, 1997). We hypothesise that fresh groundwaters on the Rottnest Island have a young meteoric origin, however the source of brackish and saline samples is less certain due to the various possible endmembers on Rottnest Island (hypersaline lakes, modern seawater or older seawater).

Production wells have been utilised since 1977 to extract water from the freshwater lens (Figs. 1A and 2B). They supply around 25% of the island's potable water and supplement water supplied by a desalination plant (Department of Water, 2014), which was commissioned in 1995 and upgraded in 2006, to meet growing demand. A number of observation wells were also installed around both freshwater lenses in the 1990s to monitor possible salinisation (Fig. 1A). Water resource use on Rottnest Island is administered by the Western Australian Government, Department of Water in accordance with the Rights in Water and Irrigation Act 1914. The Rottnest Island Authority manages groundwater abstraction on Rottnest Island and is licensed by the department to abstract up to 120,000 m^3 per year from the freshwater lens for public drinking water supply.

3. Materials and methods

3.1. Field procedures

During two field campaigns in September 2014 and March 2015, twenty-nine samples were collected from production and monitoring wells throughout the study area. Monitoring well samples were collected using a plastic submersible centrifugal pump (Supernova 120), while production well samples were collected using permanently installed production pumps. Samples were collected at, or just above the well screen, which are located at the bottom of each well, and measure a maximum of 1.5 m in length. One swamp, four lake and an ocean sample were also collected from around the study site using a peristaltic pump (Masterflex E/S portable sampler). In-field measurements including pH, temperature, electrical conductivity (EC) and dissolved oxygen (DO) were measured (YSI 556 Multiparameter Instrument). After standing water levels were measured, the monitoring wells were purged of three well-volumes and until stabilisation of in-field parameters. Production wells were purged until stabilisation of in-field parameters before groundwater samples were collected. Total alkalinity concentrations were determined by a double endpoint titration method using a HACH digital titrator at a dedicated field laboratory at the end of each day. Water levels were monitored at 30 min increments at a subset of wells for one year from September 2014–September 2015 using Solinst Gold Loggers which were corrected for barometric pressure.

Samples for anions, stable water isotopes (SWIs; ^{18}O, ^{2}H) and ^{3}H analysis were filtered through 0.45 lm filters and collected in 60 mL, 30 mL and 1 L high density poly-ethylene (HDPE) bottles, respectively, with no further treatment. Samples for cations were collected in 60 mL HDPE bottles and acidified with nitric acid (HNO_3). Dissolved Inorganic Carbon (DIC) and stable isotopes of DIC ($^{13}C_{DIC}$) samples were filtered through 0.2 lm filters, collected in 12 mL glass vials (Exetainers) and refrigerated after sampling.

Composite rainfall samples were collected on a weekly basis from May 2013–March 2015 in a rainfall collector designed to collect samples for isotopic analysis by preventing evaporation (Gröning et al., 2012). Samples for major ions and SWIs were collected in 30 mL HDPE bottles and treated as above.

3.2. Analysis

The chemical composition of water samples were analysed at the Australian Nuclear Science and Technology Organisation (ANSTO) by ion chromatography and inductively coupled plasma-atomic emission spectroscopy for anions and cations respectively. Cations and anions were assessed for accuracy by evaluating the charge balance error, with 83% of the samples falling within ±5%. Samples with the highest errors originate from the hypersaline lakes which are not compared to endmember mixing lines.

SWIs were analysed by isotope ratio mass spectrometry (IRMS) at ANSTO and values were reported as per mil (‰) deviation from the international standard V-SMOW2 (Vienna Standard Mean Ocean Water). The ^{18}O samples were analysed using an equilibration, continuous flow IRMS method (Seth et al., 2006), while ^{2}H samples were analysed using an on-line combustion, dual-inlet IRMS method. The ^{18}O and ^{2}H measurements were reproducible to ±0.15‰ and ±1‰, respectively. $^{13}C_{DIC}$ were also analysed at ANSTO by IRMS and results were reported as per mil (‰) deviations from the international carbonate standard NBS19 ($\delta^{13}C$ = +1.95‰ VPDB) with a precision of ±0.3‰. Dissolved inorganic carbon (DIC) concentrations were calculated by a concentration calibration curve based on the methodology outlined by Assayag et al. (2006). 3

H samples were analysed at ANSTO, with water samples being distilled and electrolytically enriched prior to analysis by a liquid scintillation method. The ^{3}H concentrations were expressed in tritium units (TU) with a general uncertainty of ±0.1 TU and quantification limit of 0.06 TU.

Density was measured in the laboratory at room temperature (22.7–23 C) using an electronic density metre (Densito 30PX, Mettler Toledo, Columbus, Ohio). Density measurements are reported for a temperature of 20 C.

Saturation indices for calcite, the partial pressure of CO_2 (P_{CO2}), HCO_3 and HCO_3 complex ($MgHCO^{+}_{3}$, $CaHCO^{+}_{3}$) concentrations as well as DIC concentrations were calculated with the hydrogeochemical software PHREEQC 3, using the Pitzer database (Parkhurst and Appelo, 2013).

The correlation of all results was calculated using a Spearman's rank correlation.

3.3. Calculations and data manipulation

A number of methods were used to interpret processes occurring on Rottnest Island including a density correction for hydraulic head values, an estimation of recharge via a volumetric water balance, a Cl mass balance and renewal rate approach based on ^{3}H; and the calculation of the fraction of seawater in groundwater samples to establish mixing effects. These methods are described below.

3.3.1. Density correction

Hydraulic head values were converted to freshwater heads ($h_{f,r}$) at a reference level z_r across the freshwater lens to correct for density effects according to the following formula (Post et al., 2007):

$$\frac{\rho_i}{\rho_f} h_i - \frac{\rho_a}{\rho_f}(z_i - z_r) = h_{f,r} - z_r$$

where ρ_i is groundwater sample density, ρ_f is freshwater density, ρ_a is the average water density between elevation head, z_i, and the reference level z_r, and h_i is hydraulic head. Freshwater density was taken to be the lowest density value recorded from production wells within the freshwater lens on Rottnest Island (0.9987 g/ cm^3) and the reference level (z_r) was taken to be 4 m AHD, which was close to the average screen depth across the lens.

3.3.2. Seawater fraction

To investigate the salinisation processes, the fraction of seawater (f_{sea}) in groundwater samples was calculated using the conservative tracer, Cl according to the following calculation (Appelo and Postma, 2005):

$$f_{sea} = \frac{m_{Cl;\,sample} - m_{Cl;\,fresh}}{m_{Cl;\,sea} - m_{Cl;\,fresh}} \quad (2)$$

where f_{sea} is the fraction of seawater in a sample; and m_{Cl} is Cl concentration in a sample, freshwater end-member or seawater end-member, as denoted by the respective subscripts.

3.3.3. Lens area

The minimum spatial extent of the freshwater lens was approximated by the presence of fresh groundwater, which was determined by a comparison of hydrochemical and isotopic data and water levels from the current study. Groundwaters with TDS less than 1000 mg/L in the centre of the lens were determined to be fresh according to TDS values outlined by Fetter (2001), and therefore constitute the freshwater lens. This is the same range used by Playford and Leech (1977).

3.3.4. Renewal rate

A renewal rate approach, where the concentration of ^{3}H in groundwater at time i ($^3H_{GW(i)}$) may be predicted from ^{3}H in precipitation ($^3H_{p(i)}$), was used to estimate groundwater recharge rates on Rottnest Island (La Salle et al., 2001; Cartwright et al., 2007), according to the following equation:

$$^3H_{GW(i)} = (1 - R_n)\,{}^3H_{GW(i-1)}e^{-k} + R_n\,{}^3H_{p(i)} \quad (3)$$

where k is the decay constant (5.64 $\times$ 10^{-2}/year) and R_n is the renewal rate, which is defined as the proportion of water replaced in the reservoir each year by recharge. The calculations assume that pre-atmospheric nuclear test precipitation (pre-1959) had the same ^{3}H concentration as modern precipitation in Perth (2 TU), hence groundwater activity in 1959 is calculated for a constant input activity, $^3H_{GW}$, of 2 TU according to the following equation:

$$^3H_{GW} = \frac{}{R}\,{}^3H_{p-1} \quad (4)$$

For subsequent years, the amount weighted average ^{3}H concentration of precipitation in Perth was taken as that of local precipitation, with the ^{3}H values sourced from data collected by the Australian Atomic Energy Commission (AAEC) and ANSTO (Calf et al., 1977; Calf and Stokes, 1979, 1981, 1983, 1985, 1987; Tadros et al., 2014) and the Global Network of Isotopes in Precipitation (GNIP) database (IAEA/WMO, 2016). Data from 2008 to 2015 is previously unpublished data collected for the GNIP database by ANSTO. The record was extrapolated between 1992 and 2005 due to the absence of data.

Recharge rates relate to renewal rates via the following equation:

$$R = R_n b n \quad (5)$$

where b is aquifer thickness and n is porosity. This approach provides a coarse estimate of recharge due to the broad assumptions by which the method is applied to the lens; that the system is a well-mixed reservoir, and that the complete mixing of successive recharge events occurs within the lens. Due to vertically stratified chemistry in many aquifer systems caused by slow mixing rates, individual recharge events may only supply ^{3}H to the top portion of the aquifer. As a result, the degree of chemical stratification, and thus the effective aquifer thickness (i.e., the portion of the aquifer with which the recharging water mixes), needs to be constrained (Cartwright et al., 2007). For the current study, an effective aquifer thickness of 5 m was used and porosity values of 0.3–0.5 were assessed as a reflection of the porosity of the Tamala limestone around the Perth region (Smith et al., 2012).

3.3.5. Chloride mass balance

Groundwater recharge was also estimated using a chloride mass-balance method according to the following equation (Appelo and Postma, 2005) by:

$$R = P \frac{Cl_P}{Cl_{gw}} \quad (6)$$

where R is recharge (mm/year); P is rainfall (mm/year); Cl_P is weighted average rainfall chloride concentration (mg/L); and Cl_{gw} is groundwater chloride concentration (mg/L) from the freshwater end-member (2-90).

3.3.6. Water balance

A simplified water balance was calculated to assess how changes in climatic conditions can alter the recharge to the freshwater lens, according to the following equation:

$$R = P - ET \quad (7)$$

where R is the maximum groundwater recharge estimate, P is precipitation (mm/day) and ET is evapotranspiration rate (mm/day). Runoff was omitted from the calculation due to the highly permeable nature of the Tamala limestone and the absence of water courses. Recharge was calculated as the cumulative summation of daily P – daily ET, when P − ET > 0. ET is provided by the Bureau of Meteorology (Rottnest Island Station Number 9193) which is calculated as reference evapotranspiration (ET_o) according to the Penman-Monteith equation, as recommended by the United Nations Food and Agriculture Organisation in their Irrigation and Drainage paper 56 (FAO56) for a standardised vegetated surface (Allen et al., 1998). This estimate probably represents a maximum estimate, as water loss from the soil by ET (water deficit) during dry periods is not included.

4. Results

4.1. Rainfall

The long term average rainfall from 1880 to 2015 on Rottnest Island is 691 mm/year, however the 1965–2015 average (since the decline in rainfall in the region commenced) has fallen to 597 mm/year (BOM, 2016b). The rainfall during the monitoring period in 2014 was 456 mm, which reflects drier than average conditions. Long term rainfall trends show that more than 80% of rainfall occurs between the months of May and September, which is reflected during the current monitoring period (Fig. 3).

Table 1 shows the mean chemical and isotopic data for composite rainfall samples collected on a weekly basis between May 2013 and March 2015. Rainfall collected on Rottnest Island is dominated by Na^+ and Cl, which is typical of coastal precipitation (Blackburn and McLeod, 1983; Keywood et al., 1997), with high variability observed across samples. The isotopic composition varies from 7.38‰ to 0.99‰ for $\delta^{18}O$ and from 48.7‰ to 3.3‰ for $\delta^{2}H$ (Table 1), with local amount weighted rainfall signatures for $\delta^{18}O$ and $\delta^{2}H$ being 3.8‰ and 15.1‰ respectively. Based on this rainfall data, a Local Meteoric Water Line (LMWL) for Rottnest Island, calculated using a precipitation weighted least squares regression method (Crawford et al., 2014), is given by $\delta^{2}H = 7.02 / \delta^{18}O +$ 12.05.

4.2. Water levels and groundwater abstraction

A comparison of historic groundwater levels from the Department of Water, WA (WIN, 2015), taken from monitoring wells between 1977 and 1995, and current groundwater levels from 16 wells shows maximum fluctuations of between 0.2 and 0.5 m. No well at present shows a change in water level that, when compared to historic values, would suggest a significantly altered water table. The observed fluctuations are most likely the result of seasonal variation in recharge, abstraction and ocean level oscillations, as discussed below.

To better understand the response of the freshwater lens to tidal variations, rainfall and abstraction, groundwater levels were monitored at a number of sites on Rottnest Island (Fig. 1A) from September 2014–September 2015 and compared to sea level from Hillarys Tidal Gauge, Western Australia (BOM, 2016a), rainfall and groundwater abstraction volumes supplied by the Rottnest Island Authority (Fig. 3). The magnitude of water level variations observed in monitored wells over this period ranged from 0.28 to 0.54 m. Highest groundwater levels were observed between April and July, when ocean levels peaked, rainfall was high (average rainfall: 430 mm from April–July; 1880–2015) and groundwater abstraction had ceased. Water levels then declined in conjunction with decreasing sea level to their lowest level between November and February, which coincides with a sea level trough, as well as a period of reduced rainfall (average rainfall: 46 mm from November–February; 1880–2015) and increased groundwater abstraction (average abstraction: 18,128 m^3 from November–February; 2007–2015) (Fig. 3). Annual sea level variations in the south-west Western Australian region are attributed to changes in the strength of the Leeuwin Current (Feng et al., 2003). In a typical seasonal cycle, the Leeuwin current is strongest between June and August which results in higher sea levels, and weakest between December and February, resulting in lower sea levels, in response to the opposing southerly winds (Smith et al., 1991; Feng et al., 2003, 2013).

Groundwater levels were found to be highly responsive to daily tidal oscillations, with all monitored wells showing fluctuations of varying magnitude driven by the ocean (Fig. 3). As expected, the tidal impact on groundwater levels was most pronounced in wells closest to the ocean (5-94, 27-90, 24-90, 5-90; Figs. 1A and 3), with groundwater levels primarily controlled by ocean level. Wells located further from the coast (11-90, 15-9; Figs. 1A and 3), while still effected by tidal oscillations, did not show such large daily fluctuations.

Groundwater flow directions are constructed on the basis of water level data collected in September 2014, and corrected to

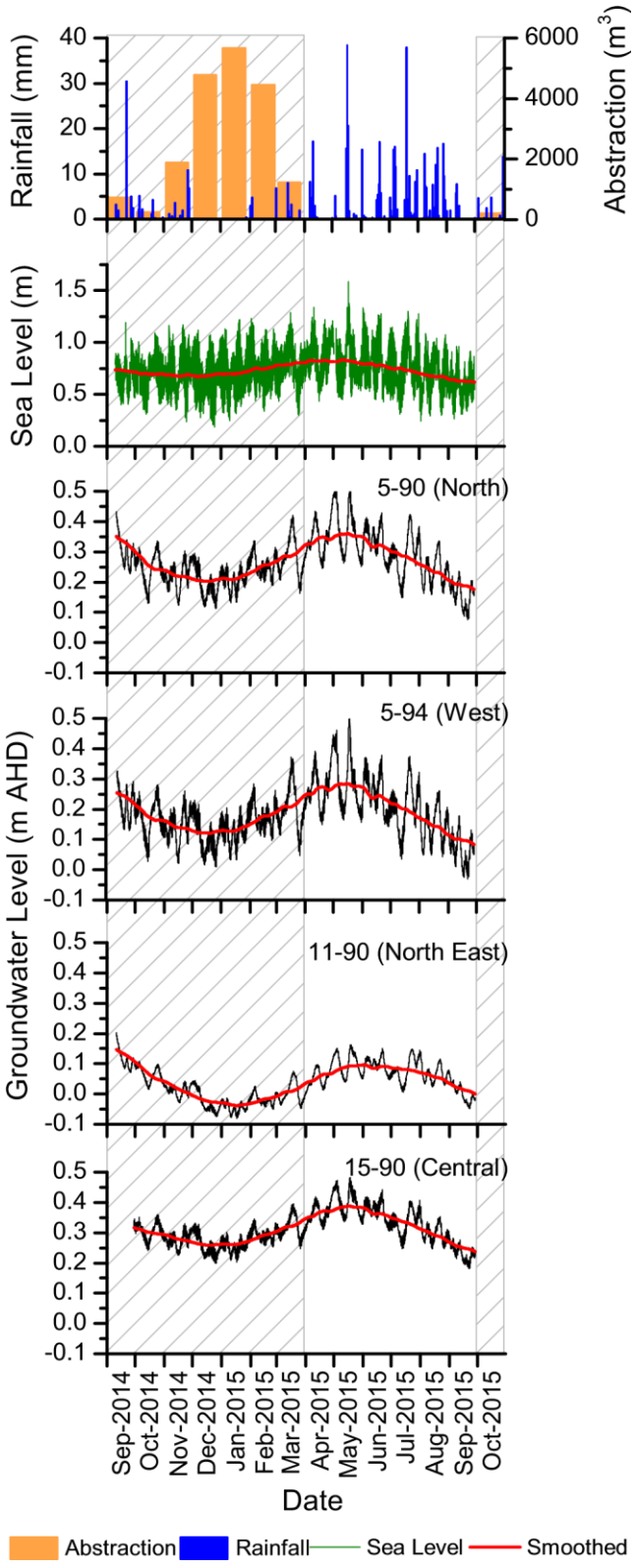

Fig. 3. Monthly abstraction rates, daily rainfall and groundwater levels (in meters Australian Height Datum: m AHD), measured from six monitoring wells from September 2014 to September 2015. Sea level fluctuations are also included from the Hillary Tidal Gauge, Western Australia (BOM, 2016a). The grey cross-hatched area indicates periods of groundwater abstraction.

freshwater heads at a reference elevation of 4 m AHD according to Eq. (1) (Post et al., 2007). The freshwater head differences between wells are small (maximum 0.62 m), which creates difficulties in accurately determining the groundwater flow directions due to the diurnal tidal variations as water levels were measured over the course of one day which encompassed one tidal period. Approximate piezometric contour lines and main groundwater flow directions are illustrated in Fig. 4, and indicate general groundwater flow towards the coast and hypersaline lakes on Rottnest Island. One well in the northern section of the study site had a freshwater head

value below sea level (0.11 m, Well 11-90) and a high TDS value (29,664 mg/L). Whilst it cannot be excluded that active seawater intrusion is causing salinisation in this part of the aquifer, it also cannot be excluded that salinities here are high due to natural processes, such as interaction with the saline lakes.

4.3. Hydrochemistry

Table 2 shows the chemical and isotopic data for groundwater and surface water samples collected in September 2014 and March 2015. Samples are divided into four types based on TDS as outlined by Fetter (2001); Fresh (0–1000 mg/L TDS), Brackish (1000– 10,000 mg/L TDS), Saline (10,000–100,000 mg/L TDS) and Brine (>100,000 mg/L TDS). Groundwater salinity ranged from fresh (605 mg/L TDS) to saline (29,675 mg/L TDS) and surface water samples from saline (17,833 mg/L TDS) to brine (186,692 mg/ L TDS). The spatial distribution of TDS for all samples is provided in Fig. 4, with fresher groundwater occurring in the central area of the study site, which is characterised by higher freshwater head values.

A comparison of current and historic TDS values highlight a significant increase in TDS in a number of monitoring wells situated around the perimeter of the freshwater lens since the 1990s (Table 2; Fig. 4). While higher salinity groundwaters in these areas are expected due to natural mixing processes, the 60–3000% increase in salinity suggests that the system is changing. This salinisation trend does not appear to have significantly affected the salinity of fresh groundwater abstracted by production wells within the centre of the lens except for two wells (1-90, 8-90) in the north where the salinity has increased from fresh to brackish (TDS increase of 402% and 117%, respectively) (Table 2; Fig. 4).

All groundwater samples are generally characterised by a near neutral pH (mean = 7.54, S.D. = 0.15, n = 29), while surface water samples range from pH 7.48 to pH 10.13. High pH values of surfaces waters are likely caused by photosynthetic activity in microbial mats within the lakes, which consume inorganic carbon resulting in an increased pH (Visscher and Stolz, 2005). The high pH results in CO^2_3 being a predominant species as well as HCO_3 , which explains the variation between some surface water HCO_3 and DIC values.

Most groundwater samples are dominated by Na^+ and Cl, ranging from fresh Na-Mg-Ca-Cl-HCO_3 to saline Na-Cl waters, with fresh and brackish groundwaters characterised by higher concentrations of Ca^{2+}, Mg^{2+} and HCO_3 . All surface waters have either a Na-Cl or Na-Mg-Cl water type. Groundwater major ion concentrations are generally related to well screen elevation in m AHD (Cl vs. Elevation $r^2 = 0.837$; Fig. 5A), with major ion concentrations increasing with decreasing elevation. HCO_3 is an exception, and shows an increase in concentration within fresh and brackish waters, and lower concentrations in saline groundwater (Fig. 5C). A correlation between dissolved oxygen (DO) and screen elevation is observed, with a number of brackish and saline samples at lower elevations showing DO concentrations below 0.5 mg/L, suggesting anoxic conditions (Fig. 5D). The anoxic conditions developing with decreasing elevation are believed to be a combination of longer residence time (see tritium data below) combined with the consumption of DO by organic matter oxidation.

Reactions involving major ions were investigated by comparing observed concentrations to the conservative mixing of a freshwater

Table 1
Average concentrations of major elements and water isotopes in Rottnest Island rainfall.

Analysis	Ca	K	Mg	Na	Cl	SO_{24}	HCO_3[a]	d_2H	$d_{18}O$	d-excess
Units	mmol/L	mmol/L	mmol/L	mmol/L	mmol/L	mmol/L	mmol/L	‰	‰	‰
Average S.D.	0.12 0.09	0.05	0.20 0.15	1.78 1.30	1.98	0.13	0.06	10.2	3.2	15.6
		0.04			1.62	0.11	0.06	11.2	1.5	3.5
Minimum	0.03	0.01	0.03	0.28	0.34	0.03	0.00	48.7	7.4	4.1
Maximum	0.39	0.14	0.60	5.35	7.33	0.52	0.20	3.3	1.0	22.9
Number	25	25	25	25	52	52	25	52	52	52

[a] Concentration estimated by difference.

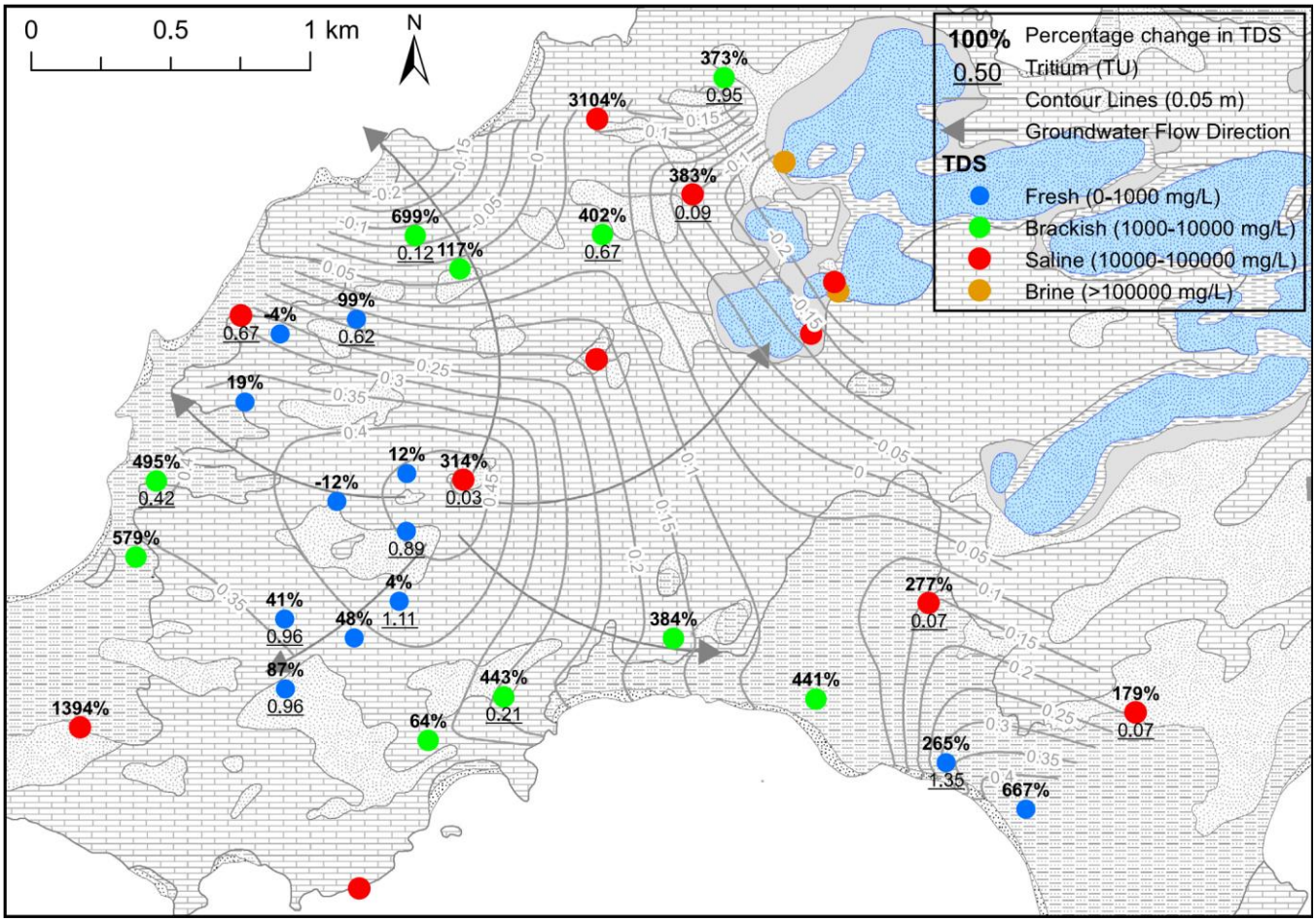

Fig. 4. Contour plot showing freshwater head values in September 2014 around the freshwater lens and groundwater flow directions towards the coast and lakes. Also indicated are the TDS classification (refer to Fig. 1 for well numbers and surficial geology), according to the water types defined by Fetter (2001) as well as the percentage change in groundwater TDS from 1977 to 2014 (bold text). A positive % change in groundwater TDS reflects salinisation, while a negative % change in groundwater TDS reflects freshening of the groundwater (historic TDS values are also provided in Table 2). ^3H concentrations are also provided where available (underlined values).

and seawater end-member. The freshest production well sample (2-90) was used as the freshwater end-member, while a surface seawater sample (SW) was collected from the coast of the Island and used as the seawater end-member. While very similar to the composition of standard seawater, the local seawater sample was used as a more representative indication of the surrounding marine environment. Most Cl-major ion relationships are predominantly linear and generally reflect the conservative mixing line (Fig. 6A–F), however an excess of Ca^{2+} and HCO_3 ions and a deficit of SO^2_4 ions is observed in some samples, including in anoxic samples. Brackish waters in particular show elevated HCO_3 concentrations compared to the conservative mixing line (Fig. 6F).

All groundwater samples are close to equilibrium with respect to calcite (mean = 0.11, S.D. = 0.11, n = 29), and fall within the combined analytical error of ±0.2, while all surface waters are supersaturated with calcite (mean = 1.1, S.D. = 0.36, n = 6).

4.4. Environmental isotopes

The isotopic composition of groundwaters range from 4.47‰ to 0.36‰ for $d^{18}O$ and from 20.0‰ to 1.5‰ for d^2H. The d^2H-$d^{18}O$ relationship for all samples was compared to the GMWL, given by $d^2H = 8 / d^{18}O + 10$ (Craig, 1961), the Perth LMWL, given by $d^2H = 6.7 / d^{18}O + 9.5$ (unpublished data collected by ANSTO), and

the Rottnest LMWL, given by $d^2H = 7.02 / d^{18}O + 12.05$ (Fig. 7A). The Rottnest Island LMWL lies next to the LMWL for the Perth Region, which was expected due to their close proximity.

Table 2
Field parameters and concentrations of major elements and environmental isotopes.

ID	Sample type[a]	Sample date	Screen elevation (m AHD)[b]	T[c] (C)	pH	DO[d] (mg/L)	Density (g/cm^3)	TDS[e] (mg/L)	Historic TDS[f] (mg/L)	Ca_{2+} (mmol/L)	Mg_{2+} (mmol/L)	Na^{+} (mmol/L)	K_{+} (mmol/L)	Cl (mmol/L)	SO_{24} (mmol/L)	HCO_{s} (mmol/L)	Sr_{2+} (mmol/L)	CBE[g] (%)	Water type	f_{seah}	d_2H (‰)	$d_{18}O$ (‰)	d-excess[i] (‰)	^{3}H (TU)	$d_{13}C$ (‰)	DIC[j] (mmol/L)
2-77 3-77	Prod	29/09/2014	0.11 0.01	18.5	7.6	1.8	0.9988	672	870 560	1.02	1.66	4.25	0.14	4.55	0.47	4.49	0.03	1.0	Na-Mg-Ca-Cl-HCO_3	0.00	18.2	4.31	16.28	0.89	7.0 8.2	4.72
1-83	Prod	29/09/2014	0.09	15.9	7.5	1.5	0.9989	776	650	1.25	2.05	4.53	0.13	5.06	0.65	5.21	0.03	1.3	Na-Mg-Ca-HCO_3-Cl	0.00	19.5	4.23	14.34	0.96	8.6	5.59 4.96
4-83	Prod	28/09/2014	0.11	16.5	7.5	1.6	0.9989	789	490 539	1.35	1.84	4.92	0.13	6.13	0.64	4.65	0.04	2.5	Na-Mg-Ca-Cl-HCO_3	0.00	17.4	3.82	13.21	1.11	5.9	4.47 5.39
1-90	Prod	30/09/2014	0.90	16.8	7.8	4.2 2.5	0.9988	674	401	1.05	1.95 3.84	3.78	0.13	4.44	0.66	4.29	0.04	0.6	Mg-Na-Ca-Cl-HCO_3	0.00	18.2	3.96	13.48	0.67	6.7	4.16 4.83
2-90	Prod	29/09/2014	0.50	15.9	7.5	3.6 3.4	1.0003	2461	528	1.88	1.54 1.63	26.42	0.62	35.06	1.04 0.41	5.07	0.05	4.6	Na-Cl	0.00	17.2	3.98	14.64	0.62	6.5	6.67 5.65
6-90	Prod	29/09/2014	0.64	18.5	7.8	1.9	0.9987	605 799	434 533	1.02	2.57	3.57 5.36	0.10	4.24 6.75	0.46 0.97	4.00	0.02 0.02	1.4	Na-Mg-Ca-Cl-HCO_3	0.00	17.7	4.21	15.98	0.96	8.6	4.68 4.41
8-90	Prod	29/09/2014	0.59	18.6	7.7	1.3	0.9988	1144	698	1.47 1.45	1.90	8.89	0.13 0.26	9.24	0.54	4.61 6.19	0.03	2.5	Na-Mg-Ca-Cl-HCO_3	0.00	19.6	4.29	14.72	0.96	7.3	4.81
16-90	Prod	29/09/2014	0.28	18.8	7.4	3.5	0.9992	812	745 860	1.57	2.02	4.71	0.14	5.91	0.74	5.24	0.04	0.5	Na-Mg-Cl-HCO_3	0.00	16.3	4.11	16.58	0.09	9.8	8.13
17-90	Prod	28/09/2014	0.06	16.8	7.4	2.9	0.9989	787	2310	1.17	2.02	5.05	0.15	5.93	0.66	4.52	0.04	1.6	Na-Mg-Ca-Cl-HCO_3	0.00	16.6	3.92	14.76	0.21	8.6	3.86
3-93	Prod	30/09/2014	0.27	16.7	7.9	4.0	0.9989	833	6150 920	1.17 1.17	1.68	6.06	0.13	7.52	0.42	4.17	0.03	1.4	Na-Mg-Cl-HCO_3	0.00	17.9	3.87	13.06	0.03 0.07	5.9	3.75
6-93 5-90	Prod	29/09/2014	0.22	18.7	7.6	0.4	0.999	713	5550 6700	3.93	10.52	4.33	0.12	5.48	3.31	4.57	0.02	1.6	Na-Mg-Ca-Cl-HCO_3	0.00	20.0	4.28	14.24	0.12	5.8	7.23
7-90	Prod	29/09/2014	6.90 7.06 6.19	16.6	7.6	3.3	0.9988	6868	740	6.81	31.48	93.34	1.95	97.02	16.35	7.51	0.13	1.4	Na-Cl Na-Cl	0.01	19.1	4.47	16.66 3.80	0.67	2.3	3.21
11-90	Mon	27/09/2014	3.55	17.3	7.3	0.5	1.0043	20,676	740	9.58	41.75 7.59	275.43	5.64	320.86	23.01 2.86	3.65	0.06	1.6	Na-Cl	0.00	17.7	3.76	7.04 0.36	0.09	3.1	4.01
13-90	Mon	12/03/2015	14.92	22.3	7.4	0.5	1.014	29,675	970 650	2.50	32.89	383.69	8.04	473.24	16.16	3.57	0.13	3.5	Na-Cl	0.17	5.6	1.58	14.94	0.21	7.3	7.00
15-90 18-90 21-90	Mon	26/09/2014	11.16	18.6	7.5	0.2 0.3	1.0254	4997	420	7.14 7.44	37.90	59.33	1.19	74.12	20.45	6.42	0.08	5.5	Na-Cl	0.57	1.4	0.36	2.12 1.30	0.03 0.07	4.1 2.9	5.81
	Mon	11/03/2015	4.04	20.1	7.2	0.3	1.002	22,977	5860 130	2.90	5.61	282.81	6.55 7.67	380.99	3.76	3.04	0.26	0.0	Na-Cl Na-Cl	0.84	17.7	4.08	3.94		5.9 9.0	4.33
24-90	Mon	26/09/2014	3.47	19.4	7.5	0.4	1.0154	25,267	230	1.48	2.62	311.96	1.06	409.13	1.11	3.78	0.06	2.8	Na-Cl	0.13	17.7	3.76	3.98 2.46		7.4	5.22
25-90 27-90 28-90	Mon	27/09/2014	14.92	17.8	7.4	0.3	1.0175	3584	160	4.86	22.19	38.46	0.28	46.38	11.19	6.47	0.03	3.3	Na-Cl Na-Cl	0.68	5.6	1.58	1.43 3.81		7.3	5.23
	Mon	26/09/2014	11.16	19.1	7.4	0.9	1.0012	1211	175	6.99	32.33 2.60	9.02	3.93	11.87	17.47 0.67	5.48	0.04	6.4	Na-Mg-Cl-HCO_3	0.73	1.4	0.36	2.32		4.1 2.9	4.20
31-90	Mon	26/09/2014	4.04	19.4	7.6	1.1	0.9993	14,489		2.20	25.58	187.87	6.12	224.96	14.22	4.11	0.10	3.3	Na-Cl Na-Cl	0.08	17.7	4.08	4.34 4.20	0.95	5.9 9.0	4.79
1-94	Mon	27/09/2014	3.47	17.5	7.5	0.3	1.01	20,824		7.69	1.34	288.46	0.53	308.92	0.37	4.85	0.10	6.4	Na-Cl Na-Cl	0.01	9.1	2.12	4.13	0.07	7.4	3.72
2-94	Mon	26/09/2014		19.0	7.3	4.6	1.0159	1986		1.52	0.70	20.61	4.55	27.36	0.29	4.89	0.04	5.6	Na-Ca-Mg-HCO_3-Cl	0.40	5.1	1.30	4.27		2.2 3.0	5.29
3-94	Mon	26/09/2014		20.0	7.5	7.1	0.9999	16,344		1.45	2.03	217.12	0.11	244.19	0.73	4.01	0.06	3.3	Ca-Na-Mg-HCO_3-Cl	0.55	18.1	3.94	4.38 4.34	1.35	9.8	5.99
4-94	Mon	28/09/2014	4.98	18.4	7.6	3.0	1.0122	667		1.80	2.79	3.73	0.08	4.55	1.04	4.58	0.01	5.6	Na-Mg-Cl-HCO_3 Na-Mg-Cl-HCO_3	0.04	18.5	3.98	5.27 2.72		9.4	5.24 2.91
5-94	Mon	28/09/2014	1.52 9.20	18.7	7.7	2.4	0.9989	474		1.40	2.64	2.27	0.25	2.68	1.17	3.52	0.01	1.2		0.43	11.2	2.46				1.58
LV	Mon	28/09/2014	0.53 1.00 0.72	19.2	7.6	1.1	0.9987	1244		1.28	175.08	10.81	0.20	13.68	74.85	4.99	0.01	3.3	Na-Mg-Cl-HCO_3	0.00	5.8	1.43	5.39	0.67		2.19 3.87
LS	Mon	27/09/2014	1.83	17.6	7.6	4.4	0.9993	1075		24.60	107.06	7.32	0.24	8.90 8.85	66.30	5.69	0.05	4.4	Na-Cl Na-Cl	0.00	16.9	3.81	0.40	0.42		2.41
PL	Mon	27/09/2014	1.87	17.5	7.6	2.4	0.9992	1040		28.04	146.31	7.54	34.03	1524.00	76.66	5.01	0.06	2.0	Na-Cl	0.02	8.9	2.32				2.11
LB	Mon	27/09/2014		18.6	7.7	5.2	0.9992	102,355		25.96	298.15	1555.00	20.33	1025.30	150.87	2.18	0.26	1.6	Na-Cl	0.01	19.1	4.34				
BS	Lake	30/09/2014		16.7	8.4	1.7	1.0872	69,331		30.05 4.71	33.13	986.51	27.13	1196.80	20.07	0.81	0.36	1.0	Na-Mg-Cl	0.01	17.7	4.20				
SW	Lake	30/09/2014		15.4	9.0	14.6	1.0566	85,146		10.12	54.23	1313.90	54.79 5.21	3216.30	31.35	1.53	0.39	3.7	Na-Cl	2.73	16.5	4.13				
	Lake	30/09/2014		16.5	8.6	6.7	1.0745	186,692				2572.60	10.48	258.25		3.36	0.37	2.3		1.84	18.2	4.27				
	Lake	12/03/2015		28.0	7.5		1.1246	17,833				234.93		560.56		0.43	0.20	1.7		2.14	19.5	4.38				
	Swamp	29/09/2014		23.1	10.1		1.0138	35,780				480.74				1.95	0.07	8.4		5.77	9.1	1.68				
	SW	12/03/2015		21.2	8.1		1.0216											4.8		0.46	13.9	2.40				
																		10.9		1.00	9.4	1.52				
																		3.6								
																		2.1			15.9	2.66				
																		0.5			5.2	0.70				

[a] Prod = Production, Mon = Monitoring, SW = Sea Water.

[b] Australian Height Datum.

[c] Temperature.

[d] Dissolved Oxygen.

[e] Total Dissolved Solids.

[f] Historic values collected between 1977 and 1994.

[g] Charge Balance Error.

[h] Seawater Fraction.

[i] Deuterium Excess.

[j]

Dissolved Inorganic Carbon.

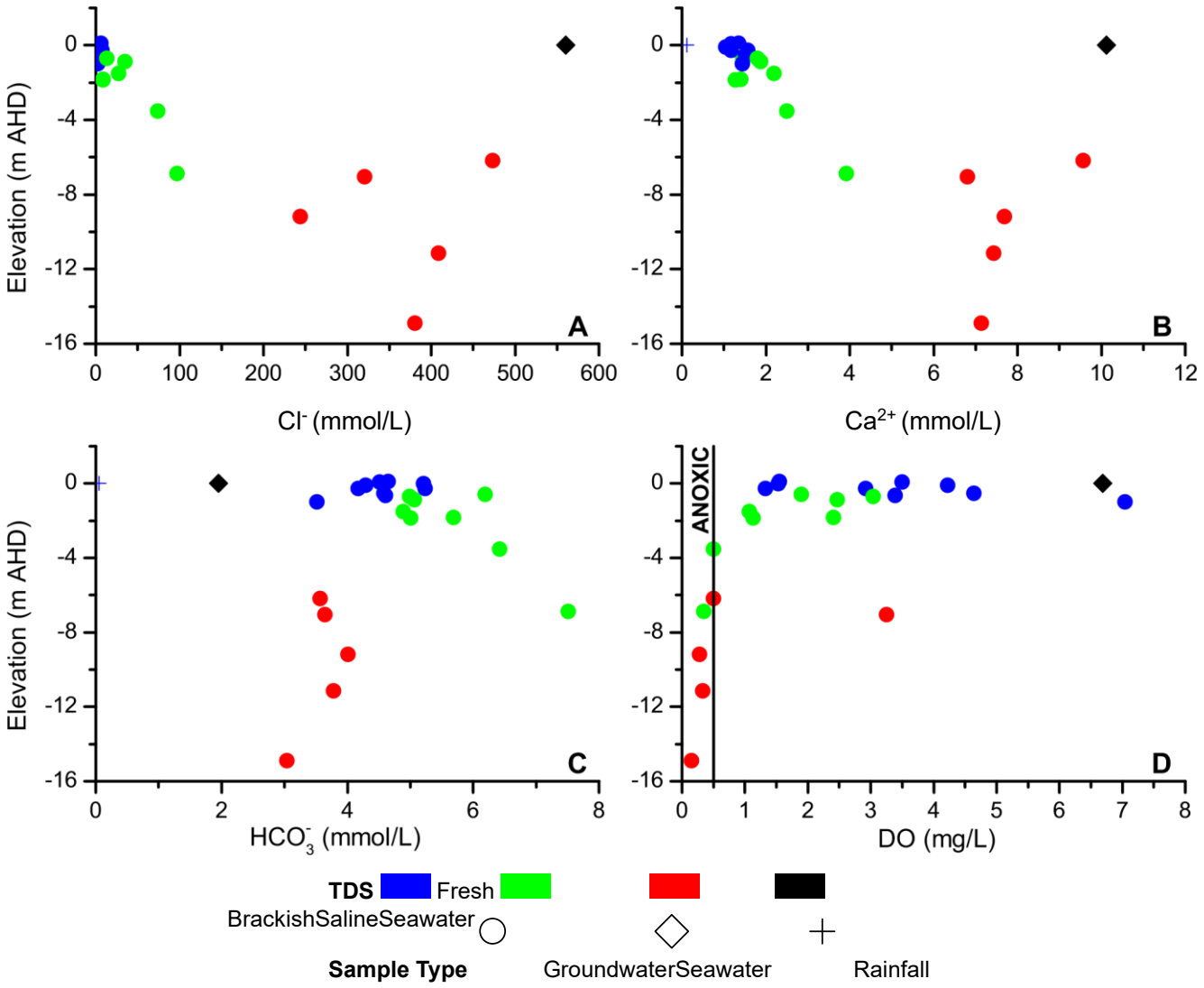

Fig. 5. Bivariate plots showing elevation compared to (A) Cl, (B) Ca^{2+}, (C) HCO_3 and (D) Dissolved Oxygen (DO) for groundwaters and seawater.

All fresh and brackish groundwaters fall on the Perth LMWL and are isotopically similar to rainfall samples collected on Rottnest Island. These results support the assumption that fresh groundwaters have a predominantly rainfall origin, with the saline portion of brackish samples resulting from either seawater mixing or salts dissolved by rainfall derived from dry deposition. Saline groundwater values are more enriched relative to rainfall and deviate away from both the Rottnest and Perth LMWL and towards the surface seawater sample, which suggests that simple mixing is the predominant influence on the isotopic composition of these saline waters. Surface waters are further enriched in $d^{18}O$ and $d^{2}H$ compared to groundwater samples and seawater, with the enrichment trend associated with increasing Cl concentration.

The deuterium excess (d-excess), given by $d = d^{2}H - 8 / d^{18}O$, provides information regarding precipitation sources and evaporative processes occurring within the system (Dansgaard, 1964). Groundwater d-excess values range from 1.5‰ to 16.7‰, while surface water d-excess values range from 5.4‰ to 0.4‰. A comparison of d-excess and Cl further emphasises the isotopic enrichment trend occurring in increasingly saline samples, with a linear trend observed between fresh groundwaters and seawater ($r^2 = 0.63$). Surface waters do not follow this trend and show more varied isotopic values (Fig. 7B).

Fresh groundwater $d^{13}C_{DIC}$ values range from 11.0‰ to 5.8‰, while brackish and saline groundwater samples range from 11.0‰ to 2.3‰ and from 9.4‰ to 2.2‰ respectively (Table 2). All samples are depleted compared to seawater (0.9‰), and show some enrichment with decreasing depth (data not shown). Surface water $d^{13}C_{DIC}$ values range from 11.1‰ to 2.8‰. Groundwater $d^{13}C_{DIC}$ values do not show any correlation with DIC concentrations, which range from 3.21 to 8.13 mmol/L.

Groundwater ^{3}H concentrations range from 0.03 to 1.35 TU, with most saline samples showing ^{3}H concentrations close to or below the detection limit (0.06 TU) (Fig. 8). Measurable ^{3}H concentrations indicate that fresh and brackish groundwaters have been recharged in the last 60 years, while deeper saline groundwaters without ^{3}H may indicate older seawater below the freshwater lens (Fig. 8). ^{3}H concentrations and elevation are positively correlated ($r^2 = 0.83$; excluding the outlier), however one sample, 7-90, does not fit within the observed trend of declining ^{3}H concentration with decreasing elevation (Fig. 8). Well 7-90 is located in close proximity to the coast (110m; Fig. 4), with the likely cause of the elevated tritium concentration being modern seawater intrusion during the last decade, or mixing of older seawater (>60 years) with fresh rainfall recharge.

4.5. Lens area and recharge estimates

The extent of the freshwater lens was investigated using a hydrochemical and isotopic approach, with fresh groundwater

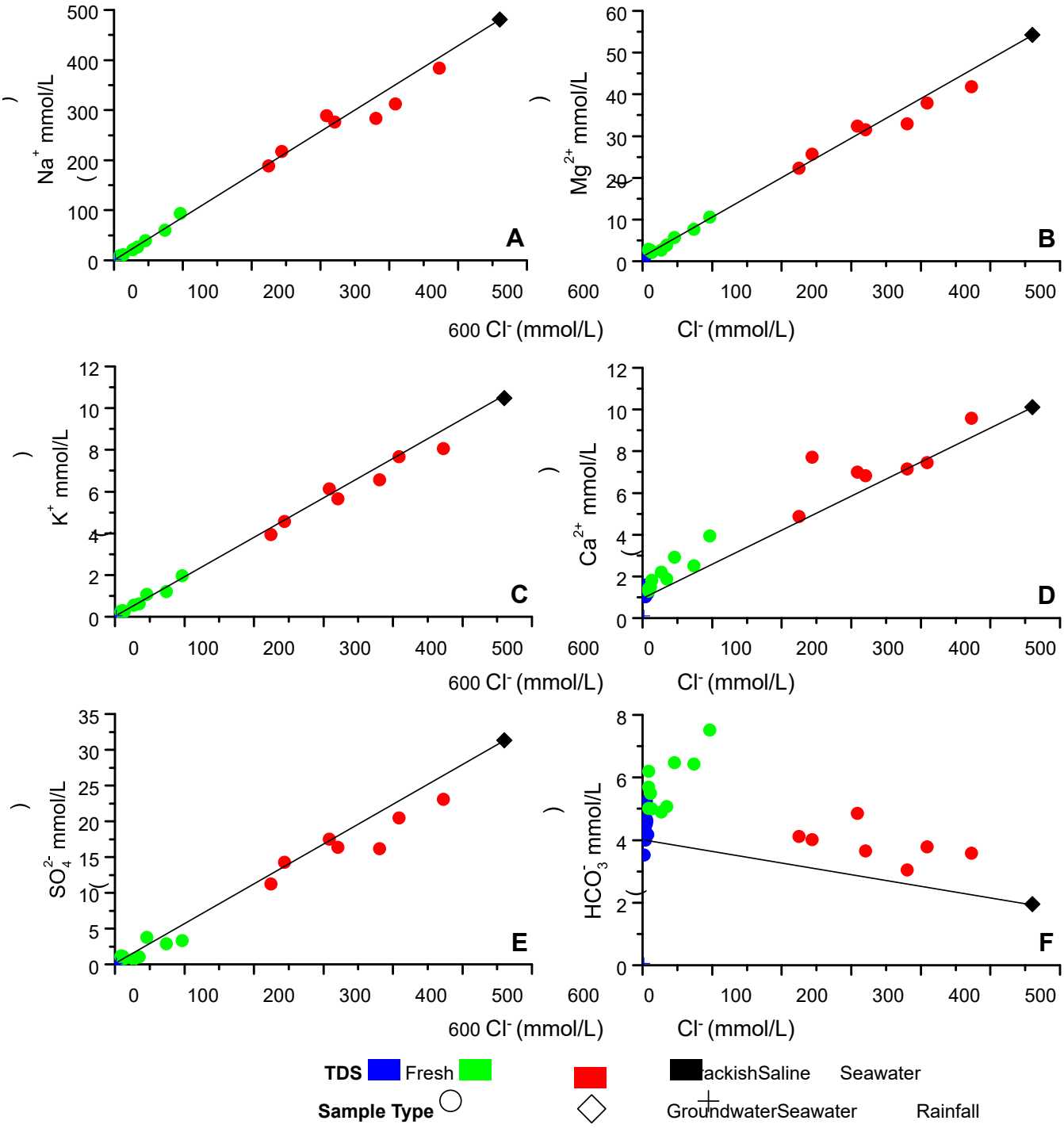

Fig. 6. Bivariate plots showing the relationship between Cl concentration and (A) Na^+, (B) Mg^{2+}, (C) K^+, (D) Ca^{2+}, (E) SO^2_4 and (F) HCO_3 compared to a conservative mixing line (black line) between a freshwater and seawater end-member.

characterised by <1000 mg/L TDS and $d^{18}O$ and d^2H values close to that of rainfall, which provides evidence of a freshwater lens that spans an area of approximately 1.6 km^2 (Fig. 4). The lens perimeter was delineated by $d^{18}O$ and d^2H enriched brackish and saline groundwaters (1049 mg/L–29,664 mg/L TDS) with a high fraction of seawater (40–83%).

As rainfall recharge is the main natural influence on the occurrence of freshwater lenses on small islands (White and Falkland, 2010) such as Rottnest Island, a comparison of three methods for assessing groundwater recharge were made. A renewal rate approach (Eqs. (3)–(5)) (Małoszewski and Zuber, 1982; La Salle et al., 2001; Cartwright et al., 2007), which uses rainfall ^3H values from Perth, Western Australia between 1955 and 2015 and groundwater ^3H activities collected from

Rottnest Island during this study was also investigated. Porosity values between 0.3 and 0.5 were used in accordance with Tamala Limestone values reported for the Perth region (Smith et al., 2012). Maximum annual recharge rates into the freshwater lens based on the aquifer renewal rates for 2014 (the year in which samples were collected) range from 147 mm to 245 mm for a porosity of 0.3 and 0.5 respectively, which represents 32–54% of rainfall on Rottnest Island in that year. Across the estimated lens area (1.6 km^2), this equates

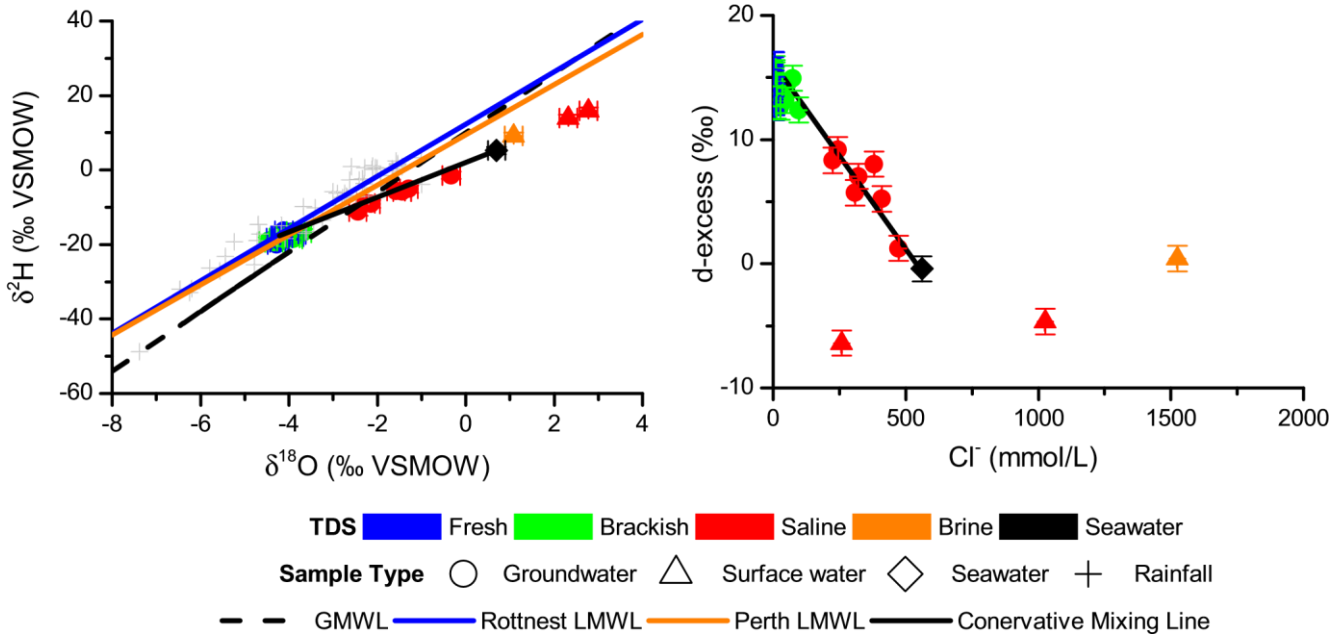

Fig. 7. Bivariate plots showing the relationship between (A) d^{18}O vs. d^{2}H from groundwaters, sea water and surface waters, and weekly rainfall samples collected between May 2013 and March 2015; and (B) Cl and deuterium excess for groundwaters, seawater and surface waters. The black line indicates conservative mixing between the fresh and seawater end-member.

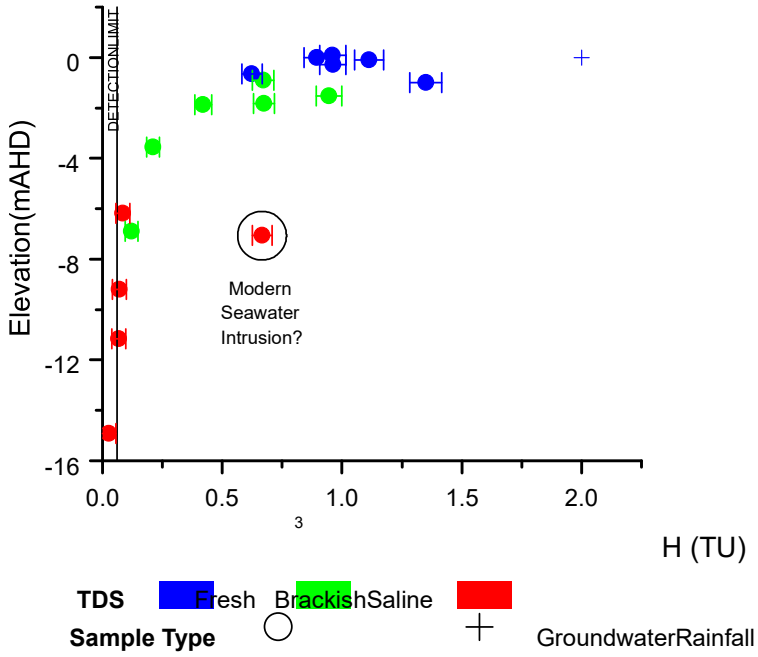

Fig. 8. Bivariate plots showing groundwater and Perth rainfall ^{3}H activity vs. screen elevation. Measurable ^{3}H concentrations indicate that fresh and brackish groundwaters have been recharged in the last 60 years, while deeper saline groundwaters without ^{3}H may indicate older seawater below the freshwater lens.

to a maximum recharge volume of 235,000–392,000 m^3 in 2014. A Cl mass balance method (Eq. (6)) suggests recharge of 267,000 m^3 across the lens area in 2014, which equates to 37% of rainfall, while the simple water balance approach (Eq. (7)) estimates a maximum recharge volume of 428,160 m^3 in 2014, which represents 59% of rainfall in that year. Groundwater abstraction over the same period was 21,366 m^3, which corresponds to between 5% and 9% of recharge for the various recharge calculation methods.

5. Discussion

5.1. Origin of the groundwater

The hydrochemical and isotopic results of groundwater samples from Rottnest Island show that while rainfall is the dominant water source, many groundwater samples are also influenced by a salinisation trend. Rainfall infiltrates rapidly into the Tamala limestone and recharges the freshwater lens, followed by lateral movement towards the coast and hypersaline lakes (Fig. 4). All groundwater samples are near saturation with calcite, with many brackish and saline samples showing an excess of Ca^{2+} and HCO_3 compared to a conservative mixing line (Fig. 6D and F) which is indicative of calcite dissolution (Plummer, 1975; Back et al., 1979, 1986; Smart et al., 1988; Stoessell et al., 1989). A Ca:HCO_3 molar ratio of approximately 1:2 for fresh groundwaters also suggests that calcite dissolution by carbonic acid is the primary waterrock interaction process after groundwater recharge into the carbonate aquifer. A general increase in $\delta^{13}C_{DIC}$ values with decreasing depth also supports this, where calcite dissolution would result in groundwaters that approach the $\delta^{13}C_{DIC}$ value of marine carbonates (0‰) (Clark and Fritz, 1997). The excess HCO_3 in brackish samples is likely caused by enhanced calcite dissolution due to mixing processes between fresh and saline waters (Wigley and Plummer, 1976; Back et al., 1986), however further investigations surrounding the carbon cycle and the hydrochemical evolution of the groundwater system on Rottnest Island will be the focus of subsequent research.

Salt water intrusion was deduced as the dominant process causing the salinisation trend (Fig. 6), which was further substantiated by the presence of enriched $\delta^{18}O$ and $\delta^{2}H$ groundwater values plotting towards the isotopic composition of seawater (Fig. 7A and B). The presence of saline (16,334–29,675 mg/L TDS), anoxic waters (<0.05 mg/L DO) below the freshwater lens without measurable tritium suggests that the saline water is older seawater (>60 years) that has mixed with older fresh waters recharged >60 years ago. One saline groundwater sample (7-90; 20,673 mg/L TDS), located 110 m from the west coast, shows higher levels of dissolved oxygen (3.26 mg/L) and has measurable ^{3}H (0.67 TU) which does not follow the trend observed in all other saline groundwaters. Weighted annual average tritium values in Perth rainfall have ranged between 1.29 TU and 33.7 TU since 1960 and reached background levels (2 TU) by 2006 (Tadros et al., 2014, and previously unpublished data collected by ANSTO for GNIP) after the bomb pulse peak in the 1960s. Since then weighted annual averages have ranged from 1.29 TU to 2.10 TU. This groundwater value (0.67 TU) is significantly lower than rainfall ^{3}H, but higher than all other saline groundwaters (0.03–0.09 TU), which may result from modern seawater intrusion in this area due to the proximity of the well to the coast (110 m), as seen in other studies (Sivan et al., 2005). The value could also result from mixing of older saline groundwater (>60 years) with fresh rainfall recharge. Current tritium data for seawater in the study region is not available, however tritium values of 2 TU were measured in the oceans around southern Australia by Tamuly (1974) in 1969/70, while a value of 3.4 TU was reported by Kakiuchi et al. (1999) off the Perth coast in 1996/97. Delineation of the contribution of modern seawater, rainfall or an older seawater source is the subject of further research, where noble gas isotopes such as ^{39}Ar are being measured and will be used to estimate the contribution of these end-members to the groundwater. Without such an approach these contributions cannot be accurately calculated. While the contributions are yet to be determined, it can be deduced from this study that older saline groundwaters (>60 years) below the freshwater lens have mixed with older fresh groundwaters (>60 years) that were not previously saline, which has resulted in a general thinning of the lens in the northern section of the aquifer (Fig. 4).

The hypersaline lakes are characterised by high concentrations of major ions (69,282 mg/L–186,613 mg/L TDS), reaching more than five times seawater composition (35,768 mg/L) due to repeated evaporation cycles (Playford, 1997; Boulton et al., 2014), and is the subject of further investigation. The $\delta^{18}O$ and $\delta^{2}H$ values of lake waters show that they do not provide any notable contribution to the groundwater (Fig. 7A and B), with lake isotopic values ($\delta^{18}O$ mean: 1.79‰; S.D.: 0.77 ‰; n = 5) being highly enriched compared to groundwater values ($\delta^{18}O$ mean: 3.51‰; S.D.: 1.13‰; n = 29). As a result, the end-members which contribute to the groundwater system on Rottnest Island are rainfall, which recharges the system and older seawater, which mixes with fresh water to produce groundwaters of increasing salinity. Further research is required to confirm the modern seawater endmember. The lakes therefore represent a zone of groundwater discharge rather than a source of potential recharge.

5.2. Reduction in lens extent

Analysis of hydrochemical, isotopic and water level results provided information to approximate the minimum spatial extent of the freshwater lens on Rottnest Island, which was determined to be 1.6 km^2. This equates to a reduction of 1 km^2 since 1977, when the lens area was estimated to be approximately 2.6 km^2 (Playford and Leech, 1977). The reduced lateral extent is supported by a comparison of historic and present day TDS values (Table 2; Fig. 4), which show increased groundwater salinity in most monitoring wells located around the perimeter of the freshwater lens, from a maximum TDS value of 6700 mg/L in 1990 to 30,000 mg/L in 2014/15. A 3000% increase in TDS in the northern section of the freshwater lens (Well 27-90; Fig. 4) since 1990 highlights the large salinity changes in this area in particular. Two production wells in the vicinity (1-90, 8-90) show slightly brackish waters (2461 mg/L and 1144 mg/L TDS, respectively), compared to 1990 values which were fresh (490 mg/L and 528 mg/L TDS, respectively). The respective screen depths of 0.90 m and 0.59 m AHD suggests that only very limited fresh water could be present above the screened interval, with further investigation required to determine if abstraction from these production wells has exacerbated saltwater intrusion in the northern area. While the extent of the freshwater lens has been reduced since 1977, saltwater intrusion has not significantly affected the salinity of fresh groundwater abstracted by production wells at the centre of the lens at this point in time (Fig. 4). The absence of detectable salt water intrusion into the centre of the freshwater lens is likely due to the position of production wells at the centre of the lens and the location of their screens (Table 2) just below the water table, which rises to a maximum of 0.51 m AHD during the current study and reduces the risk of seawater entering the wells (Barlow, 2003).

The lens was previously suggested to be around 9 m thick in the centre of the aquifer (Playford and Leech, 1977; Smith, 1994), with a mixing zone greater than 10 m thick below. Based on the freshwater head value (0.51 m) of a single deep monitoring well located at the centre of the lens area (15-90; Fig. 1A), the Ghyben-Herzberg relationship predicts a freshwater lens thickness of 20.5 m. The Ghyben-Herzberg relationship is for a sharp interface and it provides a better estimate of the 50% seawater contour (Izuka and Gingerich, 1998; Masciopinto, 2006), rather than the definition of the freshwater lens as less than <1000 mg/L TDS used in this and previous estimates. This well reveals highly saline groundwater (TDS = 22,977 mg/L) at a screen elevation of 15 m AHD, with a seawater fraction of 0.68, which suggests that the screen samples the mixing zone below the freshwater lens. Despite a stable water table across the island over the last twenty-five years, an increase in TDS from 5550 mg/L TDS in 1990 to 22,977 mg/L in 2014 was observed in this central well (15-90), which indicates that the thickness of the freshwater lens in this area is also thinning, caused by the upwards migration of older saltwater. Whether this is caused by localised upconing of saltwater or a more widespread shrinking of the lens thickness requires further investigation due to the general absence of deeper wells.

5.3. Impacts of variations in rainfall and abstraction on the lens

Three recharge estimates were applied to Rottnest Island in an attempt to deduce the impact of both abstraction and rainfall decline on the freshwater lens extent and their relationship to the observed saltwater intrusion on Rottnest Island. Each method is based on a number of assumptions, which are likely to influence the recharge value estimates to varying degrees. The renewal rate approach assumes a well-mixed reservoir and complete mixing of successive recharge events occurs within the lens, while the Cl mass balance approach is likely to underestimate recharge due to an underestimation of Cl from dry deposition captured by rainfall collectors compared to natural vegetation (Appelo and Postma, 2005), which may be significant in a coastal area such as Rottnest Island. The water balance approach is a highly simplified approach and does not consider soil moisture or corrections to potential evaporation values due to the absence of vegetation crop factors for Rottnest Island. Assumptions aside, the three methods are in general agreement and provide relatively similar approximations of recharge across the lens, which increases confidence in their use.

As the recharge estimates suggest, effective recharge on Rottnest Island ranges from 37 to 59% of rainfall, with an average of 45%. To provide a rough estimate of recharge before the decline in rainfall commenced in the late 1960s, this effective recharge value was applied to the long term rainfall average (757 mm) from 1911 to 1970, which suggests an average recharge volume of 549,667 m^3/year. Compared to effective recharge in 2014, which was drier than average, this equates to a reduction of approximately 200,000 m^3, which would lead to a decrease in the volume of water within the lens, and supports the observed reduction in both the lateral extent and thickness of the lens on the island. While groundwater abstraction has occurred since 1977, the small volume of groundwater removed from the system compared to the total volume of recharge (5–9%) is unlikely to have been a significant cause of seawater intrusion into the freshwater lens. As a result of the ongoing decrease in rainfall in the region, the Rottnest Island Authority has reduced the volume of water being abstracted from the freshwater lens over the last decade to limit potential salt water intrusion. Average annual abstraction volumes since 2005 have been approximately 33,000 m^3/year, which is significantly lower than the calculated annual volume of recharge.

Models have predicted a continued decline in rainfall in the region by approximately 40% from the 1911 to 1970 average by the late twenty-first century (Delworth and Zeng, 2014). This would lead to a reduction in recharge of approximately 218,000 m^3/year compared to the 1911–1970 average, which is a similar reduction observed during 2014, due to drier that average conditions. The seasonal variation and the effects of abstraction, combined with the continued decline in rainfall in the region, will need to be examined to better understand the impact of these factors on the extent of the freshwater lens and is the subject of our future research.

6. Conclusion

This study has advanced our understanding of a freshwater lens on a small carbonate island using hydrochemical and isotopic data measured on rainfall, groundwater and surface water. Rainfall was confirmed as the origin of fresh groundwater, while seawater mixing was identified in a number of monitoring wells around the freshwater lens. Enhanced seawater intrusion was observed in the northern section of the lens area and a reduction in the extent of freshwater was identified through a comparison of current and historic data, caused primarily by reduced rainfall in the region since the late 1960s, rather than groundwater abstraction. Saltwater intrusion by older seawater (>60 years) was identified in different regions of the lens using tritium, which supports a reduction in both the freshwater lens extent and thickness. This paper quantifies the effects of groundwater abstraction and reduced rainfall on the freshwater lens extent, and identifies that declining rainfall in the region since the late 1960s is the primary cause of the saltwater intrusion, rather than abstraction. The influence of ocean level variations on the groundwater system was highlighted through groundwater level monitoring, with further research required to further quantify the effects of seasonal fluctuations in tidal variations, groundwater abstraction and rainfall on the available freshwater resource, which is essential for the long term management of the freshwater lens. This is particularly important with the region facing a continued decline in rainfall, which has been shown to significantly impact the volume of recharge the freshwater lens receives.

Acknowledgements

The authors wish to thank the Rottnest Island Authority (RIA), especially Helen Shortland-Jones, Cassyanna Thomas, Luke Wheat and Shane Kearney for their ongoing support of this project. The authors would also like to thank Suzanne Hollins, leader of the Isotopes for Water research group at the Australian Nuclear Science and Technology Organisation (ANSTO) for her ongoing support as well as various ANSTO personnel including Robert Chisari, KellieAnne Farrawell, Barbora Gallagher, Scott Allchin, Henri Wong and Chris Vardanega for their assistance in chemical and isotopic analysis, Jagoda Crawford for assistance with rainfall SWI calculations and Chris Dimovski and Stuart Hankin for their assistance with field trip preparation. Finally we would like to thank Gabriel Rau, from the Connected Waters Initiative, UNSW, for his assistance with preparing for and processing data from an elevation survey on Rottnest Island.

References

Allen, R.G. et al., 1998. Crop Evapotranspiration – Guidelines for Computing Crop Water Requirements – FAO Irrigation and Drainage Paper 56. FAO, Rome 300 (9), D05109.
Andersen, M.S. et al., 2005. Geochemical processes and solute transport at the seawater/freshwater interface of a sandy aquifer. Geochim. Cosmochim. Acta 69 (16), 3979–3994.
Appelo, C.A.J., Postma, D., 2005. Geochemistry, Groundwater and Pollution. A.A. Balkema, Rotterdam.
Assayag, N. et al., 2006. Improved method for isotopic and quantitative analysis of dissolved inorganic carbon in natural water samples. Rapid Commun. Mass Spectrom. 20 (15), 2243–2251.
Ataie-Ashtiani, B. et al., 1999. Tidal effects on sea water intrusion in unconfined aquifers. J. Hydrol. 216 (1), 17–31.
Back, W. et al., 1986. Differential dissolution of a Pleistocene reef in the groundwater mixing zone of coastal Yucatan, Mexico. Geology 14 (2), 137–140.
Back, W. et al., 1979. Geochemical significance of groundwater discharge and carbonate solution to the formation of Caleta Xel Ha, Quintana Roo, Mexico. Water Resour. Res. 15 (6), 1521–1535.
Barlow, P., 2003. Ground water in freshwater-saltwater environments of the Atlantic coast. US Geol. Surv. Circ. 1262, 113.
Barlow, P.M., Reichard, E.G., 2010. Saltwater intrusion in coastal regions of North America. Hydrogeol. J. 18 (1), 247–260.
Barria, P. et al., 2015. Uncertainties in runoff projections in southwestern Australian catchments using a global climate model with perturbed physics. J. Hydrol. 529, 184–199.
Blackburn, G., McLeod, S., 1983. Salinity of atmospheric precipitation in the MurrayDarling drainage division, Australia. Soil Res. 21 (4), 411–434.
BOM, 2016a. Australian Baseline Sea Level Monitoring Project. Bureau of Meteorology, Australian Government. <http://www.bom.gov.au/ oceanography/projects/abslmp/abslmp.shtml> (accessed 20/07/2016).
BOM, 2016b. Australian Government Bureau of Meteorology – Climate Averages Tables, Rottnest Island <http://www.bom.gov.au/climate/averages/tables/cw_ 009193.shtml> (accessed 22/02/2016).
Boulton, A. et al., 2014. Australian Freshwater Ecology: Processes and Management. John Wiley & Sons, UK.

Brooke, B., 2001. The distribution of carbonate eolianite. Earth Sci. Rev. 55 (1), 135– 164.
Calf, G. et al., 1977. AAEC Tritium List No. 2, 1975–1976. AAEC/E414. Australian Atomic Energy Commission Research Establishment, pp. 26.
Calf, G., Stokes, R., 1979. AAEC Tritium List No. 3, 1977–1978. AAEC/E473. Australian Atomic Energy Commission Research Establishment, pp. 26.
Calf, G., Stokes, R., 1981. AAEC Tritium List No. 4, 1979–1980. AAEC/E519. Australian Atomic Energy Commission Research Establishment, pp. 24.
Calf, G., Stokes, R., 1983. AAEC Tritium List No. 5, 1981–1982. AAEC/E569. Australian Atomic Energy Commission Research Establishment, pp. 24.
Calf, G., Stokes, R., 1985. AAEC Tritium List No. 6, 1983–1984. Australian Atomic Energy Commission Research Establishment, pp. 19.
Calf, G., Stokes, R., 1987. AAEC Tritium List No. 1, 1985–1986. ANSTO/E661. Australian Nuclear Science and Technology Organisation, pp. 18.
Cant, R.V., Weech, P.S., 1986. A review of the factors affecting the development of Ghyben-Hertzberg lenses in the Bahamas. J. Hydrol. 84 (3), 333–343.
Cartwright, I. et al., 2007. Constraining modern and historical recharge from bore hydrographs, ^{3}H,^{14}C, and chloride concentrations: applications to dual-porosity aquifers in dryland salinity areas, Murray Basin, Australia. J. Hydrol. 332 (1), 69– 92.
Clark, I., Fritz, P., 1997. Environmental Isotopes in Hydrology. CRC Press, Florida, USA.
Collins, L. et al., 1991. The Abrolhos carbonate platforms: geological evolution and Leeuwin current activity. J. R. Soc. West. Austr. 74, 47–57.
Collins, L. et al., 1993. Late Quaternary evolution of coral reefs on a cool-water carbonate margin: the Abrolhos Carbonate Platforms, southwest Australia. Mar. Geol. 110 (3), 203–212.
Craig, H., 1961. Isotopic variations in meteoric waters. Science 133 (3465), 1702– 1703.
Crawford, J. et al., 2014. Alternative least squares methods for determining the meteoric water line, demonstrated using GNIP data. J. Hydrol. 519, 2331–2340. Dansgaard, W., 1964. Stable isotopes in precipitation. Tellus 16 (4), 436–468.
Davidson, W.A., 1991. Review of the Groundwater Monitoring Program for Rottnest Island Water Supply (Unpublished). Western Australia Geological Survey. Hydrogeology Report 1991/12, pp. 8.
Davidson, W.A., Mory, A.J., 1990. Prospects of Obtaining Additional Groundwater Supplies on Rottnest Island (Unpublished). Hydrogeology Report 1990/3. Western Australia Geological Survey, pp. 12.
Delworth, T.L., Zeng, F., 2014. Regional rainfall decline in Australia attributed to anthropogenic greenhouse gases and ozone levels. Nat. Geosci. 7, 583–587.
Department of Water, 2014. Rottnest Island Water Reserve: Drinking Water Source Protection Plan. Report No. WRP 148. Department of Water, Government of Western Australia, pp. 75.
Edward, D., 1983. Inland waters of Rottnest Island. J. R. Soc. West. Austr. 66(Parts 1 and 2), 41–47.
Edward, D., Watson, J., 1959. Fresh water and brackish water swamps of Rottnest Island. J. R. Soc. West. Austr. 42, 85–86.
Falkland, A., 1991. Hydrology and Water Resources of Small Islands: A Practical Guide. UNESCO Press.
Feng, M. et al., 2013. La Niña forces unprecedented Leeuwin Current warming in 2011. Sci. Rep. 3.
Feng, M. et al., 2003. Annual and interannual variations of the Leeuwin Current at 32S. J. Geophys. Res. 108 (C11), 3355.
Ferguson, G., Gleeson, T., 2012. Vulnerability of coastal aquifers to groundwater use and climate change. Nat. Clim. Change 2 (5), 342–345.
Fetter, C.W., 2001. Applied Hydrogeology. Macmillan College Publishing Inc., New York.
Fitterman, D.V., Deszcz-Pan, M., 1998. Helicopter EM mapping of saltwater intrusion in Everglades National Park, Florida. Explor. Geophys. 29 (1/2), 240– 243.
Fretwell, J.D., Stewart, M.T., 1981. Resistivity study of a coastal karst terrain, Florida. Ground Water 19 (2), 156–162.
Ghyben, W.B., 1889. Nota in verband met de voorgenomen putboring nabij Amsterdam (Notes on the Probable Results of the Proposed Well Drilling near Amsterdam). Tijdschrift het Koninklijk Instituut voor Ingenieurs, The Hague, pp. 8–22.
Gouramanis, C. et al., 2012. Holocene palaeoclimate and sea level fluctuation recorded from the coastal Barker Swamp, Rottnest Island, south-western Western Australia. Quatern. Sci. Rev. 54, 40–57.
Gozzard, J., 2011. WA Coast: Rottnest Island. Geological Survey of Western Australia, Digital Data Product.
Gröning, M. et al., 2012. A simple rain collector preventing water re-evaporation dedicated for $d^{18}O$ and $d^{2}H$ analysis of cumulative precipitation samples. J. Hydrol. 448, 195–200.
Herzberg, D., 1901. Die Wasserversorgung einiger Nordseebäder (The water supply on parts of the North Sea coast). J. Gasbeleuchtung Wasserversorgung. München 44, 815–819.
Hirschberg, K.J., Smith, R.A., 1990. A Reassessment of the Shallow Groundwater Resources of Rottnest Island (Unpublished). Hydrogeology Report 1990/61. Western Australia Geological Survey, pp. 27.
IAEA/WMO, 2016. Global Network of Isotopes in Precipitation. <http://www.iaea. org/water> (accessed 15/02/2015).
Izuka, S.K., Gingerich, S.B., 1998. Estimation of the depth to the fresh-water/saltwater interface from vertical head gradients in wells in coastal and island aquifers. Hydrogeol. J. 6 (3), 365–373.
Kakiuchi, H. et al., 1999. Tritium concentration in ocean. J. Radioanal. Nucl. Chem. 239 (3), 523–526.
Keywood, M. et al., 1997. The accession of chloride to the western half of the Australian continent. Aust. J. Soil Res. 35 (5), 1177–1189.
Kinzelbach, W. et al., 2003. Sustainable groundwater management-problems and scientific tool. Episodes-Newsmag. Int. Union Geol. Sci. 26 (4), 279–284.
La Salle, C.L.G. et al., 2001. Renewal rate estimation of groundwater based on radioactive tracers (^{3}H, ^{14}C) in an unconfined aquifer in a semi-arid area, Iullemeden Basin, Niger. J. Hydrol. 254 (1), 145–156.
Małoszewski, P., Zuber, A., 1982. Determining the turnover time of groundwater systems with the aid of environmental tracers: 1. Models and their applicability. J. Hydrol. 57 (3), 207–231.
Masciopinto, C., 2006. Simulation of coastal groundwater remediation: the case of Nardò fractured aquifer in Southern Italy. Environ. Model. Softw. 21 (1), 85–97.
Mylroie, J.E. et al., 1995. Blue holes: definition and genesis. Carbonates Evapor. 10 (2), 225–233.
Nicholls, R.J. et al., 2007. Coastal systems and low-lying areas. In: Climate Change 2007: Impacts, Adaptation and Vulnerability. Contribution of Working Group II to the Fourth Assessment Report of the Intergovernmental Panel on Climate Change. Cambridge University Press, Cambridge, UK, p. 987.
Oude Essink, G. et al., 2010. Effects of climate change on coastal groundwater systems: a modeling study in the Netherlands. Water Resour. Res. 46 (10).
Paine, J.G., 2003. Determining salinization extent, identifying salinity sources, and estimating chloride mass using surface, borehole, and airborne electromagnetic induction methods. Water Resour. Res. 39 (3).
Parkhurst, D.L., Appelo, C.A.J., 2013. Description of Input and Examples for PHREEQC Version 3-A Computer Program for Speciation, Batch-reaction, OneDimensional Transport, and Inverse Geochemical Calculations. U.S. Geological Survey Techniques and Methods. Book 6, pp. 497. <http://pubs.usgs.gov/tm/06/ a43/> (Chapter A43).
Playford, P.E., 1988. Guidebook to the Geology of Rottnest Island. Geological Society of Australia, Western Australia Division and Western Australia Geological Survey, Perth, pp. 75.
Playford, P.E., 1997. Geology and hydrogeology of Rottnest Island, Western Australia. In: Vacher, L.H., Quinn, T.M. (Eds.), Geology and Hydrogeology of Carbonate Islands. Developments in Sedimentology, vol. 54. Elsevier, Amsterdam, pp. 783–810.
Playford, P.E., Leech, R.E.J., 1977. Geology and Hydrology of Rottnest Island. Geological Survey of Western Australia, pp. 113.
Plummer, L., 1975. Mixing of sea water with calcium carbonate ground water. Geol. Soc. Am. Memoirs 142, 219–236.
Post, V., 2005. Fresh and saline groundwater interaction in coastal aquifers: is our technology ready for the problems ahead? Hydrogeol. J. 13 (1), 120–123.
Post, V. et al., 2007. Using hydraulic head measurements in variable-density ground water flow analyses. Groundwater 45 (6), 664–671.
Rippey, M., Hobbs, R., 2003. The effects of fire and quokkas (Setonix brachyurus) on the vegetation of Rottnest Island, Western Australia. J. R. Soc. West. Austr. 86 (2), 49–60.
Ritzi, R.W. et al., 2001. Explaining the thinness of the fresh water lens in the Pleistocene carbonate aquifer on Andros Island, Bahamas. Groundwater 39 (5), 713–720.
Schneider, J.C., Kruse, S.E., 2003. A comparison of controls on freshwater lens morphology of small carbonate and siliciclastic islands: examples from barrier islands in Florida, USA. J. Hydrol. 284 (1), 253–269.
Seth, B. et al., 2006. Improved reliability of oxygen isotopic analysis of water using the Finnigan GasBench II periphery of a continuous flow isotope ratio mass spectrometer by backflushing of the sampling line. Rapid Commun. Mass Spectrom. 20 (6), 1049–1051.
Sivan, O. et al., 2005. Geochemical evolution and timescale of seawater intrusion into the coastal aquifer of Israel. Geochim. Cosmochim. Acta 69 (3), 579–592.
Small, C., Nicholls, R.J., 2003. A global analysis of human settlement in coastal zones. J. Coastal Res., 584–599
Smart, P. et al., 1988. Carbonate dissolution in a modern mixing zone. Nature 335 (6193), 811–813.
Smith, A. et al., 2012. Geohydrology of the Tamala Limestone Formation in the Perth Region: Origin and Role of Secondary Porosity. CSIRO: Water for a Healthy Country National Research Flagship, Perth, WA, pp. 74.
Smith, I. et al., 2000. Southwest Western Australian winter rainfall and its association with Indian Ocean climate variability. Int. J. Climatol. 20 (15), 1913–1930.
Smith, R.A., 1982. An Assessment of the Rottnest Island Fresh Groundwater Supply. Hydrogeology Report No. 2292. Western Australia Geological Survey, Perth, pp. 69.
Smith, R.A., 1985. Effect of Pumping on ‘‘Freshwater” Seeps, Rottnest Island (Unpublished). Hydrogeology Report 2623. Western Australia Geological Survey, pp. 14.
Smith, R.A., 1994. Groundwater Exploitation and Management on a Small Semiarid Island. Water Down Under ’94, Adelaide, Australia, pp. 473–478.
Smith, R.L. et al., 1991. The Leeuwin current off Western Australia, 1986–1987. J. Phys. Oceanogr. 21 (2), 323–345.
Stoessell, R. et al., 1989. Water chemistry and $CaCO_3$ dissolution in the saline part of an open-flow mixing zone, coastal Yucatan Peninsula, Mexico. Geol. Soc. Am. Bull. 101 (2), 159–169.
Stuyfzand, P.J., 1999. Patterns in groundwater chemistry resulting from groundwater flow. Hydrogeol. J. 7 (1), 15–27.
Tadros, C.V. et al., 2014. Tritium in Australian precipitation: a 50 year record. J. Hydrol. 513, 262–273.

Tamuly, A., 1974. Dispersal of tritium in southern ocean waters. Arctic, 27–40.
Taylor, R.G. et al., 2013. Ground water and climate change. Nat. Clim. Change 3 (4), 322–329.
Vacher, H.L., 1997. Introduction: varieties of carbonate islands and a historical perspective. In: Vacher, H.L., Quinn, T.M. (Eds.), Geology and Hydrogeology of Carbonate Islands. Developments in Sedimentology. Elsevier, Amsterdam, pp. 1–33.
Vacher, H.L., Mylroie, J.E., 2002. Eogenetic karst from the perspective of an equivalent porous medium. Carbonates Evapor. 17 (2), 182–196.
Visscher, P.T., Stolz, J.F., 2005. Microbial mats as bioreactors: populations, processes, and products. Palaeogeogr. Palaeoclimatol. Palaeoecol. 219 (1), 87–100.
Werner, A.D. et al., 2013. Seawater intrusion processes, investigation and management: recent advances and future challenges. Adv. Water Resour. 51, 3–26.
White, I., Falkland, T., 2010. Management of freshwater lenses on small Pacific islands. Hydrogeol. J. 18, 227–246.
Wigley, T., Plummer, L., 1976. Mixing of carbonate waters. Geochim. Cosmochim. Acta 40 (9), 989–995.
WIN, 2015. Water INformation (WIN) Database – Discrete Sample Data. Water Information Section, Department of Water, Perth, Western Australia. <http:// wir.water.wa.gov.au> (accessed 01/03/2015).
Yakirevich, A. et al., 1998. Simulation of seawater intrusion into the Khan Yunis area of the Gaza Strip coastal aquifer. Hydrogeol. J. 6 (4), 549–559.